Seasonal variability in the source and composition of particulate matter in the depositional zone of Baltimore Canyon, U.S. Mid-Atlantic Bight

Prouty, N.G.; Mienis, F.; Campbell, P.; Roark, E.B.; Davies, Andrew; Robertson, Craig; Duineveld, G.C.A.; Ross, S.W.; Rhode, M.; Demopoulos, A.W.J.

Deep Sea Research I: Oceanographic Research Papers

DOI:
10.1016/j.dsr.2017.08.004

Published: 01/09/2017

Peer reviewed version

Seasonal variability in the source and composition of particulate matter in the depositional zone of Baltimore Canyon, U.S. Mid-Atlantic Bight

Prouty[1*], N.G., Mienis[2], F., Campbell[1], P., Roark[4], E.B., Davies[5], A.J., Robertson[5], C.M., Duineveld[2], G., Ross[6], S.W., Rhode[7], M., Demopoulos[8], A.W.J.

Highlights

- Vertical transport and lateral transport across the continental margin were the dominant processes driving seasonal input of particulate matter
- *n*-alkane and sterol biomarker results combined with isotopes and trace metals, offers a multi dimensional approach for deciphering organic matter sources
- Elevated Chlorophyll-*a* and sterol concentrations and contemporaneous increase in the particle reactive micronutrients during the spring sampling period capture seasonal influx of relatively fresh phytodetritus.
- Connectivity to adjacent watershed facilitates offshore transport of "aged" terrestrial organic matter and nutrients

Seasonal variability in the source and composition of particulate matter in the depositional zone of Baltimore Canyon, U.S. Mid-Atlantic Bight

Prouty[1*], N.G., Mienis[2], F., Campbell[1], P., Roark[4], E.B., Davies[5], A.J., Robertson[5], C.M., Duineveld[2], G., Ross[6], S.W., Rhode[7], M., Demopoulos[8], A.W.J.

[1] US Geological Survey, Pacific Coastal and Marine Science Center, 2885 Mission Street, Santa Cruz, CA 95060 nprouty@usgs.gov
[2] NIOZ Royal Netherlands Institute for Sea Research and Utrecht University, P.O. Box 59, 1790 AB Den Burg The Netherlands
[4] Department of Geography, Texas A&M University, College Station, TX 77843
[5] School of Ocean Sciences, Bangor University, Menai Bridge Anglesey, LL59 5AB, UK
[6]University of North Carolina-Wilmington, Center for Marine Science, 5600 Marvin Moss Ln, Wilmington, NC 28409
[7] 518 McEnery Ally, Charleston, SC 29412
[8] US Geological Survey, Wetland and Aquatic Research Center, 7920 NW 71st St., Gainesville, FL 32653
**corresponding author*

Abstract

Submarine canyons are often hotspots of biomass due to enhanced productivity and funneling of organic matter of marine and terrestrial origin. However, most deep-sea canyons remain poorly studied in terms of their role as conduits of terrestrial and marine particles. A multi-tracer geochemical investigation of particles collected yearlong by a sediment trap in Baltimore Canyon on the US Mid-Atlantic Bight (MAB) revealed temporal variability in source, transport, and fate of particulate matter. Both organic biomarker composition (sterol and *n*-alkanes) and bulk characteristics ($\delta^{13}C$, $\Delta^{14}C$, Chl-*a*) suggest that while on average the annual contribution of terrestrial and marine organic matter sources are similar, 42% and 52% respectively, marine sources dominate. Elevated Chlorophyll-*a* and sterol concentrations during the spring sampling period highlight a seasonal influx of relatively fresh phytodetritus. In addition, the contemporaneous increase in the particle reactive micronutrients cadmium (Cd) and molybdenum (Mo) in the spring suggest increased scavenging, aggregation, and sinking of phytodetrital biomass in response to enhanced surface production within the nutricline. While tidally driven currents within the canyon resuspend sediment between 200 and 600 m, resulting in the formation of a nepheloid layer rich in lithogenic material, near-bed sediment remobilization in the canyon depositional zone was minimal. Instead, vertical transport and lateral transport across the

continental margin were the dominant processes driving seasonal input of particulate matter. In turn, seasonal variability in deposited particulate organic matter is likely linked to benthic faunal composition and ecosystem scale carbon cycling.

Keywords
Submarine canyons; deep-sea ecosystems; sediment trap; geochemical analyses; organic matter

1. Introduction

Submarine canyons play a key role in modulating the flux of particulate organic and inorganic matter to the deep ocean, particularly given that continental shelves and slopes are productive and dynamic ocean margin systems. As a result, canyons are often conduits for the transport of sediments, organic matter, and contaminants from continental margins to the abyssal plain, providing effective connections between highly productive shelf waters and the food limited deep-sea (Canals *et al.*, 2006; Palanques *et al.*, 2006; Costa *et al.*, 2011; Levin and Sibuet, 2012; Puig *et al.*, 2012). Contemporary sedimentary processes within canyons include storm induced turbidity currents, advection through shelf resuspension, slope failures, internal waves, trawling, and dense shelf cascading (see review by Puig *et al.*, 2014). Through the channeling and concentrating of organic matter via dynamic physical processes, canyon fauna can experience enhanced food supply (Vetter and Dayton, 1998; Duineveld *et al.*, 2001; De Leo *et al.*, 2010). Therefore, submarine canyons can potentially be hotspots of biodiversity where enhanced fluxes of organic matter and deposition sustain tremendous benthic biomass in the deep sea compared with nearby open slope habitats at similar depths (Levin *et al.*, 2001; Garcia *et al.*, 2007; De Leo *et al.*, 2010). Within canyons, different physical regimes can substantially alter the organic composition of sediments and the abundance of fauna thriving on these resources. For example, local deposition centers of sediment and organics are hotspots of detritivorous bottom dwelling organisms in the Portuguese Nazaré and New Zealand's Kaikoura canyons (De Leo *et al.*, 2010). Furthermore, episodic events known to affect benthic biomass and biodiversity, such as sediment cascades enriched in organic matter (Canals *et al.*, 2006), or increased seasonal productivity in surface waters due to upwelling along canyon edges (Soltwedel, 2000; Garcia *et al.*, 2007; Howatt and Allen, 2013), can temporarily trigger increased sedimentation and/or food availability.

Submarine canyons are a major feature incising the United States Atlantic continental margin, from Cape Hatteras to Atlantic Canada. In this region, canyons act as conduits and reservoirs of shelf-sourced sediments, transporting this material from the shelf to the slope. The MAB shelf within or near

canyons is known for high organic inputs resulting from enhanced surface water productivity (Schaff *et al.*, 1992; DeMaster *et al.*, 1994; Rex and Etter, 2010). This region also contains a high diversity of unique habitats within a relatively small area, some recognized as rich coral habitats and important areas for the diversity of the MAB (Hecker, 1980; Hecker *et al.*, 1983). The MAB is incised by 13 major canyons of varying size, shape, and morphological complexity (Obelcz *et al.*, 2014). Baltimore Canyon represents one of the best studied canyons in this region (e.g., Gardner, 1989a, b) and was the focus of a multi-year study to better understand the unique hard bottom and soft-sediment communities within and adjacent to the canyon (Brooke and Ross, 2014; Brooke *et al.*, 2016). Recent results from Baltimore Canyon have identified discrete resuspension and deposition zones in the upper canyon and the deeper part of the canyon, respectively. Differences in benthic infaunal communities of Baltimore Canyon appear to be linked to this zonation, as previously documented in other canyon and margin settings where benthic community patterns vary with depth and organic matter (OM) content (e.g., (Carney *et al.*, 2005; Gibson *et al.*, 2005; Wei *et al.*, 2010). For example, in Baltimore Canyon reduced infaunal diversity and enhanced infaunal density observed at 900 m was coincident with a zone of organically enriched, finer sediments, characterizing the depositional zone (840 to 1180 m) of the lower reaches of the canyon. In addition to spatial patterns of sediment deposition and organic composition, temporal variations in the transport of both marine and terrestrial organic matter can impact benthic community composition and trophic status (Pusceddu *et al.*, 2009), as well as the deep-sea carbon cycle through changes in ingestion, assimilation, and respiration (e.g., Vetter and Dayton, 1998; Hunter *et al.*, 2013). For example, Hunter et al. (2013) observed changes in macrofaunal feeding activity and bacterial C uptake as a result of changes in particulate organic matter (POM) composition. Therefore seasonal variations in organic matter flux are key factors influencing deep-sea ecosystems (Gooday, 2002).

A major aim of this study is to better understand the provenance signature of particle (food) delivery within a submarine canyon by analyzing a suite of geochemical tracers (e.g., stable and radio-isotopes, lipid biomarkers, ^{210}Pb, trace metals) collected during a 1-year sediment trap deployment and CTD profiling. While an arsenal of biomarker compounds (e.g., *n*-alkanes, sterols, fatty alcohols, fatty acids, lignin phenols) exist to identify biotic sources as well as yield information on decomposition and diagenesis (e.g., Bianchi and Canuel, 2011 and references therein), ambiguities do exist when elucidating sources of organic matter based on biomarker composition given overlapping sources (e.g., Volkman *et al.,* 2008). Therefore, combining the *n*-alkane and sterol biomarker results with the other tracers (i.e., stable isotopes, trace metals, radiocarbon) presented here offers a multi dimensional

approach for deciphering organic matter sources (e.g., Wakeham and McNichol, 2014). By building on previous research demonstrating the utility of hydrocarbons as tracers of organic matter source in the aquatic ecosystem (e.g., Volkman, 1986; Meyers, 1994; Goni *et al.*, 1997; Wakeham *et al.*, 1997; Eglinton and Eglinton, 2008; Wakeham and McNichol, 2014), we can investigate the primary sources of organic matter within Baltimore Canyon. Taken together this detailed study highlights for the first time key observations describing the temporal variability of organic matter flux that influences the deep-sea ecosystems within Baltimore Canyon

2. Materials and Methods

2.1 Study Area: Baltimore Canyon

Baltimore Canyon, a shelf-sourced canyon is located approximately 125 km southeast of the entrance to Delaware Bay, extends for a distance of 25 km until it merges onto the abyssal plain at a depth of 1500 m (Fig. 1). Near the head of the canyon, the width is 3 km and increases to 8 km at the shelf break at a depth of 100 m. Several meanders characterize the canyon, with the canyon axis curving southward at the upper reaches and then turning eastward with increasing depth until it is oriented east-west at 3000 m water depth (Obelcz *et al.*, 2014) (Fig. 1). A series of bathymetric steps and terraces are found near the head of the canyon where the cross-sectional profile is V-shaped and transitions into a U-shaped canyon at 1000 m (Obelcz *et al.*, 2014).

Sediment supply to Baltimore Canyon is from the pelagic zone and reworked shelf sediment (Gardner, 1989b) mainly transported via off-shelf spill in canyon heads, failure of the steep canyon walls, and resuspension by bottom currents and internal waves (Obelcz *et al.*, 2014), as well as small-scale mass wasting events triggered by bioerosion (Valentine *et al.*, 1980). Within the canyon, currents focused by the canyon axis in the form of tidal bores and internal waves resuspend sediment between 200 and 600 m and sometimes down to 800 m allowing these sediments to be transported down canyon along density surfaces (Gardner, 1989a, b). Resuspension occurs primarily during flood and to a lesser extent during ebb flows and is most intense and episodic when the water is poorly stratified (i.e., during late winter and early spring), though episodic events may occur at other times of the year (Gardner, 1989a, b).

2.2 Sediment Traps

Two benthic landers, each consisting of an aluminum tripod frame approximately 2 m in height equipped with twin acoustic releases and eight buoyancy spheres were deployed on September 5, 2012

at a depth of 603 m (38° 09.024 N, 73° 50.954 W, described as the shallow lander) and at 1318 m (38° 02.543 N, 73° 44.153 W, described as the deep lander) (Fig. 1). Each lander was equipped with a Technicap PPS 4/3 sediment trap programmed to rotate a 250 mL sample bottle at either 20 or 30-day intervals, delivering 12 samples during the 1-year deployment. Temperature, salinity, turbidity, dissolved oxygen, and bottom currents were measured using an Aanderaa (RCM) string logger. All RCM probes were mounted approximately 1.5 m off bottom with the exception of the current meter, which was approximately 2 m off the bottom. In addition, a mooring was deployed August 18, 2012 at 1082 m (38° 04.657 N, 73° 46.957 W, described as the mid-mooring) (Fig. 1). The mooring was equipped with a Honjo Parflux sediment trap with thirteen 500 mL bottles mounted 4 m above bottom programmed to rotate on a 30-day interval. The sampling design enabled the examination of canyon characteristics, including the movement of particulate material up and down canyon, propagation of internal waves, water parameter variability, and particle fluxes.

Biological activity in the sediment traps was inhibited by treating the traps with a pH buffered solution of mercuric chloride ($HgCl_2$) in seawater, which has been shown to be an effective means to limit microbial activity and subsequent alteration of organic matter (e.g., Lee *et al.*, 1992). While not immune to diagenesis/degradation within the water column (e.g., Wakeham *et al.*, 1997; Tolosa *et al.*, 2003), the retention of a "biological heritage" of lipid extraction (e.g., *n*-alkanes and sterols) from sediments is less sensitive to alteration and degradation and represents important organic geochemical proxies that are preferentially preserved relative to other classes of biomarkers (see reviews by Volkman, 1986; Meyers, 1994; Eglinton and Eglinton, 2008). Early on Prahl *et al.* (1980) demonstrated a decrease in aliphatic hydrocarbon distribution in surface sediments relative to trap sediment. Similarly, previous work has demonstrated the preferential removal of labile components and enrichment of residual recalcitrant matter in surface sediment relative to trap material (e.g., Wakeham and Canuel, 2006; Wakeham and McNichol, 2014).

The complete time-series from the shallow (603 m) and mid-depth (1082 m) trap sites were compromised by mass flux events (in October 2012) that filled the trap funnels completely, leaving only a few samples intact. The flux estimate may be unreliable since the elevated current speeds surpass the settling velocity of particles (Knauer and Asper, 1989). The only sediment trap with an almost complete sampling series was retrieved from the deepest Baltimore Canyon lander site (1318 m). The missing dates represent sediment trap bottles that were partially open upon retrieval, therefore precluding accurate flux measurements and sample preservation. Sediment trap samples were split

into five equal splits with a rotor splitter at the Royal Netherlands Institute for Sea Research (NIOZ). Two splits were rinsed thoroughly to remove sea salt and $HgCl_2$, after which they were frozen, freeze dried, and weighed to calculate mass fluxes and prepared for geochemical analyses. To keep samples intact for pigment analysis, another split was rinsed with filtered seawater from the deployment site after which it was freeze dried.

2.3 Water column properties

Vertical profiles were made of the water column properties using a CTD-rosette (SBE 911*plus* CTD profiler and a rosette containing twelve 5 L Niskin bottles) deployed inside Baltimore Canyon to establish if the canyon acts as conduit for suspended and dissolved material. One CTD transect was taken down the axis of the canyon, and during these casts, the CTD array was lowered from the surface to as close to the bottom as feasible (usually about 10 m above bottom) (Fig. 1). Seawater samples were collected during the upcast of the CTD at shallow (250 m), mid (644 m), and deep (1140 m) sites within Baltimore Canyon, as well as at mid-depth shelf sites (678 m) outside the canyon for measurements of nutrient concentrations, trace metals, and POM (>0.45 μm). Seawater was filtered directly from the Niskin bottles using acid-cleaned Teflon coated tubing attached to a polypropylene filter holder that was preloaded with an acid-cleaned polysulfone filter and attached to a vacuum pump. Filters were pre-cleaned by soaking in trace metal grade HCl in a 1 L low-density polyethylene bottle. Replicate water samples were collected from two 5 L Niskin bottles at each sampling depth. Water column particulate matter for trace element measurements was collected by filtering approximately 5 L of seawater on acid-cleaned 0.45 μm polysulfone filters (47 mm) given low blank concentrations (Planquette and Sherrell, 2012). The filter holders with preloaded filters were double bagged in polyethylene zip-lock bags and kept frozen for transport back to the laboratory.

Seawater samples collected for dissolved nutrient analysis were stored in acid-cleaned high-density polyethylene 20 mL scintillation vials, which were triple washed with extra filtrate before saving the final sample for analysis. These samples were frozen immediately until analyzed at the Geochemical and Environmental Research Group at Texas A&M University, College Station. Nutrient samples were analyzed on an Astoria-Pacific auto-analyzer. The nitrate/nitrite/silicate methods are based on Armstrong *et al.* (1967). Phosphate methods are based on Bernhardt and Wilhelms (1967). Ammonium methods are based on Harwood and Kühn, (1970). The dissolved inorganic nitrogen (DIN) concentrations were calculated as the sum of nitrite, nitrate, and ammonium concentrations. Analytical

detection limits were 0.01 μM for phosphate, 0.003 μM for nitrite, 0.05 μM for nitrate and silicate, and 0.08 μM for ammonium.

2.4 Geochemical Analyses

Sediment organic carbon and nitrogen content were measured on a Thermo Organic Elemental Analyser Flash 2000, and stable carbon and nitrogen isotopes were measured on a Thermo Delta V Advantage Isotope Ratio MS at NIOZ. Prior to analysis, samples for C_{org} and $\delta^{13}C$ analysis were acidified with HCl to remove all inorganic carbon. Standards used for C were acetanilide and benzoic acid, respectively (analytical detection limits $\delta^{13}C$ =0.3‰). Samples for %N and $\delta^{15}N$ analysis were not acidified and standards used were acetanilide and urea respectively (analytical detection limits $\delta^{15}N$ =0.1‰). Trace element concentrations of the suspended particulate matter and sediment trap material were determined by ICP-MS at the USGS Mass Spectrometry Facilities in Denver, Colorado. Filters were digested following procedures outlined in Planquette and Sherrell (2012). Data presented here were reported in μg g^{-1} following blank correction, as determined from digesting procedural filter blanks, and sample and filter weight corrections (Prouty *et al.*, 2016). For the sediment traps, 50 to 100 mg of sediment was digested using a 4-acid procedure (HF + HCl + HNO_3 + $HClO_4$), taken to dryness, and the residue dissolved in 5 to 20 mL of 5% to 13% HNO_3 with a dilution factor of 10^3 to 10^4 (Briggs and Meier, 2002).

Concentrations of chlorophyll *a* and its derivatives (phaeophorbides, phaeophytines) were determined with reverse-phase HPLC according to the method outlined by Witbaard *et al.*, (2000). Phytopigments were identified and quantified using a library based on pigment standards (DHI, Denmark). From the results of the pigment analysis, intact chlorophyll-*a* concentrations were taken as a proxy for fresh phytodetritus biomass. The chlorophyll-*a*/phaeopigment ratio was used to indicate the freshness of the trapped phytodetritus. The activity of ^{210}Pb was determined by alpha spectrometry from ^{210}Po using a Canberra alpha detector, which was extracted from the sample by leaching with concentrated HCl (Boer et al., 2006). The ^{210}Pb activity of sediment trap samples was used as an indicator for the relative proportion of suspended and freshly settled material. Fresh settled material has a high ^{210}Pb signal, while resuspended material shows lower values due to radioactive decay.

Sediment radiocarbon (^{14}C) ages were determined at the National Ocean Sciences Accelerator Mass Spectrometry (NOSAMS) facility, Woods Hole, MA USA. Approximately 50 mg of acidified (1.2N HCl) bulk sediment was converted to CO_2 and graphitized for accelerator mass spectrometry (AMS)

(Vogel *et al.*, 1987). Radiocarbon ages were calculated using the Libby half-life of 5568 years. The $D^{14}C$ values (i.e., radiocarbon values without age correction) were age corrected to account for decay that took place between collection (or death) and the time of measurement using the following equation: $\Delta^{14}C = (Fm*\text{age correction})-1)*1000$ where age correction is defined as exp((1950-year of measurement)/8267), and Fm is fraction modern (Stuiver and Polach, 1977). Radiocarbon results are reported as $\Delta^{14}C$ (‰) and conventional radiocarbon age after applying a measured $\delta^{13}C$ correction (Stuiver and Polach, 1977).

Molecular composition of the sediment trap samples was determined by gas chromatography-mass spectrometry (GC-MS) at the USGS Pacific Coastal Marine Science Center's (PCMSC) Organic Geochemistry laboratory in Santa Cruz, California as described in Prouty *et al.* (2016). Approximately 1-2 g of freeze-dried organic matter was extracted by pressurized solvent extraction (ASE, Dionex Corp., CA, USA). Samples were extracted with a hexane:acetone (1:1) solvent mixture followed by a second extraction in dichloromethane:methanol (2:1) solvent mixture. Internal standards (5-α-androstane, 5-α-androstan-3-β-ol) were added to samples prior to extraction. All glassware was washed, solvent rinsed (methanol, hexane, and dichloromethane), and combusted at 400°C overnight. Blanks were run for the entire procedure, including extraction, solvent concentration, and purification. After evaporation of extracts to 5 ml volume utilizing TurboVap Evaporation Concentrator (Zymark Corp., NC,USA), samples were loaded onto liquid chromatography columns for compound class separation. Each column was layered with 2.5 g of 5% deactivated alumina, 2.5 g of 62 silica gel and 5.0 g of 923 silica gel, which had previously been activated at 500^{o} C for 8 h and then, in the case of the alumina, partially deactivated with ultrapure water (5% w/w). Three separate fractions were collected: F1-saturate (100% hexane eluent); F2-aromatic (30% DCM : 70% hexane eluent); and, F3-polar (50% ethyl acetate: 50% hexane) and reduced in volume to 1.0 ml. The polar fraction (F3) was further derivatized with BSTFA (N,O-bis(trimethylsilyl) trifluoroacetamide) containing 2% TMCS (trimethylchlorosilane) and anhydrous acetonitrile. Extracts were analyzed by splitless injection onto an Agilent 6890 gas chromatograph interfaced to an HP 5973 mass spectrometer (GC-MS) at the USGS PCMSC Organic Geochemistry Laboratories in Santa Cruz, CA. The gas chromatograph oven program had an initial temperature of 90°C which was held for 4.0 min then ramped at 5°C min $^{-1}$ to a final temperature of 310°C which was held at this final temperature for 10 min. The capillary column (DB-5MS: 30 m length, 0.25 mm id with a 25 μm phase thickness) was directly interfaced to the ion source of the mass spectrometer. Hexane instrument blanks and procedural sample duplicates were run and analyzed for every 10 samples. Compound identifications were made by comparison with

known analytical standards and/or published reference spectra (Fig. S1). Concentrations of individual lipids are blank corrected values. Lipid biomarkers (sterol and *n*-alkane) concentrations (μg g^{-1}) are reported normalized to organic carbon of dry sediment as measured by a coulometer at the PCMSC.

Major organic matter sources to the sterol and *n*-alkane molecular signatures were investigated by calculating relative proportions of marine, terrestrial, and anthropogenic/petroleum contributions. Relative contributions from natural (marine versus terrestrial) and anthropogenic organic matter *n*-alkane and sterol sources were calculated following a modified designation from Pisani *et al.* (2013). Terrestrial organic matter composition of sediments was quantified using concentrations of odd-numbered *n*-alkanes in the C_{21} to C_{31} range as well as the sterols campesterol, stigmasterol, β-sitosterol and stigmastanol (the reduced from of stigmasterol). Marine components were determined using concentrations of the sterols cholesterol, 22-dehydrocholesterol, brassicasterol, and cholestanol (reduced form of cholesterol) as well as odd- and even-numbered *n*-alkanes in the C_{15} to C_{19} range. The anthropogenic components were determined using the sterol composition of coprostanol, epicoprostanol, and the ketone, 5-β-coprostanone, in addition to the isoprenoid hydrocarbons pristane and phytane.

3. Results and Discussion

3.1 Environmental and Water Column Variability

The three benthic observatories positioned throughout the canyon recorded decreases in current speed, turbidity, and temperature with depth (Fig. 2). The shallow lander (603 m) was positioned in the most dynamic area of the canyon, with temperatures fluctuating between 4.5- 8.6 °C and a mean of 5.4 °C (standard deviation [SD] 0.47 °C). The intensity of the current also varied greatly, with peak current velocity reaching 66.2 cm s^{-1} and a mean of 13.7 cm s^{-1} (SD 9.03 cm s^{-1}). Peaks in turbidity appeared to correspond with temperature fluctuations (Spearman's Rank Correlation on 24 hour moving average data for first deployment, $r = 0.48$, $p < 0.001$). In contrast, the mid-mooring area (1082 m) was cooler (temperatures between 4 °C-5.1° C and a mean of 4.5 °C [SD 0.16 °C]) and had a lower current velocity (maximum current velocity: 42.3 cm s^{-1}, and mean: 8.7 cm s^{-1} [SD 5.6 cm s^{-1}]). Current velocity and temperature were positively correlated at the mid-mooring location (Spearman's Rank Correlation on 24 hour moving average data for first deployment, $r = 0.43$, $p < 0.001$). The deeper region of Baltimore Canyon (1318 m) was cooler and had lower current velocities (temperatures between 3.8-4.74 °C with a mean of 4.2 °C [SD 0.16 °C]) relative to the shallower deployments. Maximum current velocity was 29.2 cm s^{-1}, with a mean speed of 6.6 cm s^{-1} [SD 3.27 cm s^{-1}]. At the

deep site, peaks in turbidity were positively correlated with current velocity (Spearman's Rank Correlation on 24 hour moving average data for first deployment, $r = 0.62$, $p < 0.001$), and there was a strong positive relationship between current velocity and temperature (Spearman's Rank Correlation on 24 hour moving average data for first deployment, $r = 0.75$, $p < 0.001$), consistent with the patterns recorded by the shallow and mid-canyon instruments. All sites indicated that warmer, sediment-laden waters are transported to the deeper parts of the canyon during part of the tidal cycle. Current driven bed shear stress (>0.1 N m^{-2}) was calculated from the sediment density and grain size, as well as the kinematic viscosity and density of the seawater. Based on this calculation, sediment remobilization varied throughout the canyon, with current driven bed shear stress sufficient to resuspend fine-grained material (i.e. <34 μm) 15% of the time at the shallow area of the canyon, but only 1% at the mid canyon and less than 0.02% in the deeper area. Plots of progressive current vectors demonstrated a strong tidal flow at the shallow lander station, with a general movement towards the northeast, up canyon. However, some disruption to this pattern was observed during certain periods throughout the year when flow moved down canyon (Fig. 1). The canyon walls steered water movement within the mid-canyon station, but disruption to the general up-canyon movement was detected during September to November and January to March (Fig. 1b). During the periods of October to November 2012 and March to May 2013, turbidity events in the shallow lander site were followed by a 2 °C temperature increase, and accentuated by elevated current speeds and flow to the north (Fig. S2), suggesting a possible link to benthic storms associated with Gulf Stream meanders and rings (Gardner *et al.*, 2017). This signal was less distinct in the deeper sites where temperature fluctuations were substantially smaller. The deep lander had the most consistent residual flow that was identical in direction to the shallow station (Fig. 1a and c). However, such transport was less tidally regulated than in the shallow station demonstrating a greater movement to the northeast.

The CTD transects conducted in Baltimore Canyon reveal a large intermediate nepheloid layer extending from the mouth of the canyon from 200 m to approximately 900 m (Fig. 3), with enhanced turbidity during both up and down canyon flow. This nepheloid layer was also observed by Gardner, (1989a, b), and likely forms a permanent feature in Baltimore Canyon in response to internal wave energy at tidal frequencies. The nepheloid layer, between 400 and 800 m, and a second, smaller patch in the surface water near the canyon wall (8 km down canyon) (Fig. 3), was characterized by increased lithogenic material, specifically aluminum (Al), neodymium (Nd), Iron, (Fe), and lanthanum (La) (Fig. 4). Particulate (>0.45 μm) element concentrations were enriched at the shallow (NF-2012-138; 261 m) and mid-depth (NF-2012-128; 644 m) CTD stations whereas trace element profiles at the deep (NF-

2012-130; 1140 m) and slope (NF-2012-149; 668 m) CTD stations did not exhibit elevated trace metal particulate concentrations at 600 m (Fig. 4). Trace element composition for the Baltimore Canyon slope site was consistently low and the deep site only showed a slight enrichment near the bottom (NF-2012-130; 1140 m). These results indicate that the nepheloid layer appears restricted to within the canyon and to a depth of 850 m.

Nutrient profiles in Baltimore Canyon displayed surface-water depletion and bottom-water enrichment in nitrate, phosphate, and dissolved silicate (Fig. 5). These results illustrate the uptake of nutrients within the nutricline due to biological processes, particularly the growth of phytoplankton in the photic zone. The interaction between phytoplankton growth and nutrient uptake is illustrated in the inverse relationship between the nutrient and dissolved oxygen (O_2) profiles (Fig. 5). Below the mixed layer, concentrations of nitrate, phosphate, and dissolved silicate were conservative and exhibited a homogenous distribution at depth. The nutricline in Baltimore Canyon was defined from nutrient profiles collected during the August 2012 sampling cruise. Maximum nutrient concentrations occurred at ~250–300 m, consistent with the thermocline depth in Baltimore Canyon, and agrees with those derived from Ocean Data Viewer (latitude 73° 49.36 N, longitude 38°23.24 W; Schlitzer, 2016). Given the similarity between the individual depth profiles down canyon, the nutricline appears to be homogenous along the length of the canyon with little spatial variability.

3.2 Sediment Traps

The sediment trap data at the deep site illustrate a narrow range of mass fluxes during the first seven months (4.7 to 9 g m^{-2} d^{-1}) and slightly lower mass flux during the last three months (Fig. 6). There were two periods of relatively elevated mass flux, September−October 2012 and January−February 2013. The increase in mass flux in September−October 2012 at the deep trap site indicates a resuspension or mass-wasting event, potentially, linked to increase mass fluxes at the shallow and mid-depth sites, and subsequent overfilling of the funnels at these shallower depths. Similar sediment trap overfilling was observed in Nazare Canyon, in response to storm-induced turbidity currents (Martín *et al.*, 2011). However, we did not observe overfilling at the deep sediment trap site, suggesting that sediment loading in the shallow and mid-depth regions may not necessarily be transported along the canyon thalweg to the deeper region, and that localized overspill from the canyon walls can help explain asynchronous mass fluxes within the canyon. At the deep trap site, percent C_{org} and total N did not vary significantly between periods and patterns of C and N fluxes and therefore closely resembled those of the mass flux, with a small range in C:N ratios (8.8 to 10.6) (Table 1). ^{210}Pb activity at the

deep trap site displayed an inverse temporal pattern relative to mass flux. Higher mass fluxes corresponded to low ^{210}Pb values (R=-0.90), indicating trapping of resuspended material (Fig. 6a). Chlorophyll-*a* concentrations showed more variability between successive samples. Peak Chl-*a* flux occurred in May−June 2013, coincident with elevated $\%C_{org}$ values and highest Chl- *a* /phaeopigment ratio, indicating a supply of relatively fresh phytodetritus from the spring phytoplankton bloom (see below). A secondary peak in Chl- *a* flux and ^{210}Pb was observed in October−November 2012, indicating enhanced transport of phytodetritus (Fig. 6b).

There was a narrow range in stable carbon ($\delta^{13}C$) and nitrogen ($\delta^{15}N$) isotope values -22.8‰ (SD 0.15) and 4.83‰ (SD 0.23) (Table 1), consistent with a marine signature (Meyers, 1994). The $\delta^{13}C$ range was consistent with that reported for POM in the surface and mid-water depths, and $\delta^{15}N$ values were consistent with surface POM values on the Northwest Continental Shelf (Oczkowski *et al.*, 2016). The trap material most likely reflects a combination of freshly exported material and suspended POM. Romero-Romero *et al.* (2016) were able to use stable isotope signatures to distinguish organic matter sources in the Aviles submarine canyon. However, in our study it was difficult to distinguish between a mixture of marine algae plus terrestrial C3 plants given the narrow range of sediment trap bulk $\delta^{13}C$ values (-22.8 to -22.0 ‰). The enriched C:N ratios relative to the Redfield ratio (6.7; Table 1) suggests a mixture of sources of both marine phytodetritus and land-derived organic debris. As shown in Figure 7, the sediment trap samples fall along a mixing line between marine algae and C3-vascular plants according to $\delta^{13}C$ and C:N values (Goñi *et al.*, 2003; Tesi *et al.*, 2007).

The total concentration of *n*-alkanes for sediment trap samples from the deep lander site represents a resolved *n*-alkane range from C_{14} to C_{32} as well as detectible amounts of the isoprenoid hydrocarbons pristane (pr) and phytane (ph) (Table 2a). Total *n*-alkane concentrations ranged from <1 to 12 $\mu g\ g^{-1}$ dry weight normalized to organic carbon ($\mu g\ g^{-1}$ C), with September/October 2012 yielding elevated *n*-alkane concentrations (Fig. 6b). Overall, the molecular composition was dominated (95%) by higher molecular weight (HMW, $>C_{21}$) *n*-alkanes, particularly *n*-C_{29} and *n*-C_{27}, except in February 2013 when *n*-C_{24} was anomalously elevated (Table 2a). The Carbon Preference Index (CPI) is often used to identify organic matter source by describing the molecular distribution of odd number *n*-alkanes relative to even number *n*-alkanes (Bray and Evans, 1961). Overall, there was a strong odd-to-even predominance, with a CPI consistently >1.0, particularly in September/October and June/July (Table 2a), suggesting increased OM originating from land plant material (Hedges and Parker, 1976). The dominance of terrestrial plant input relative to aquatic macrophytes is also expressed through the

Alkane Proxy (Paq) (Ficken *et al.*, 2000). The Paq values were consistently <1, revealing the dominance of long chain-length *n*-alkanes. Phytane was detected in the samples from September/October of 2012, but was absent from the other months. The sediment trap sample from May 2013 contained enriched pristane relative to the other months, but overall both pristane and phytane concentrations were <1 μg g^{-1} C (Table 2a). Total sterol concentrations ranged from 1 to 30 μg g^{-1} C (Table 2b), and were dominated by cholesterol. In comparison, the smallest contribution was from the anthropogenic-sourced sterols, specifically coprostanol and epicoprostanol. Sterol concentrations were elevated in October 2012 when cholesterol contributed 30% of the total sterol concentration. A second peak in sterol concentration occurred in May 2013 and was dominated by both cholesterol and cholestanol, comprising over 60% of the total sterol composition. Both sterols have marine biological sources, such as biosynthesis of plankton organisms and zooplankton (Volkman, 1986). The sterol enrichment in the spring is tightly coupled to the peak in Chl-*a* concentrations (Fig. 6b), illustrating the influx of relatively fresh phytodetritus. The influx of fresh phytodetritus is also consistent with the phytoplankton blooms in the spring when net primary productivity exceeded 700 g C m^{-2} d^{-1} (Fig. 6d), as calculated per Behrenfeld and Falkowski (1997) for a 20 km^2 surrounding Baltimore Canyon. In comparison, lower sterol and *n*-alkane concentrations during the winter months reflect a reduction in surface water primary productivity (< 300 g C m^{-2} d^{-1}) during the winter season.

The distribution of biomarkers in the sediment trap organic matter indicates that delivery to the deep area of Baltimore Canyon is a composite of sources (e.g., algal/phytoplankton/zooplankton productivity and land-plant productivity). Anthropogenic sources were minimal, with an annual average contribution of 6%, and the greatest contribution occurring in September 2012. Although high pristane concentrations in sediment can be derived from zooplankton, the pristane/phytane ratios observed in this study are used as indicators of a petrogenic, anthropogenic source (Blumer *et al.*, 1963). While on average the contributions from marine (43%) and terrestrial (52%) organic matter sources were similar, seasonal variability in source contribution was observed in the biomarker time series (Table 3). For example, September 2012 and May 2013 were dominated by terrestrial (76%) and marine (71%) sources, respectively. Dominance by terrestrial sources in September 2012 was potentially associated with a resuspension event as captured in the increased mass flux and reduced ^{210}Pb values, and potentially linked to enhanced turbidity from overspill of the canyon walls. In contrast, the peak in marine sources in May 2013 is attributed to increased primary production during the spring bloom (Fig. 6d), when freshwater transport is at a maximum during spring discharge (Choi

and Wilkin, 2007), and facilitates offshore transport of both nutrients and terrestrially derived organic matter.

A suite of trace elements was measured from the sediment trap samples collected at the deep lander site (Table 4). Iron (Fe) and aluminum (Al) dominated the trace element composition of the sediment traps, but showed little variability throughout the deployment period with average monthly Fe and Al concentrations of 56 and 32 mg g^{-1}, respectively. After Fe and Al, barium (Ba), phosphorous (P), strontium (Sr), and manganese (Mn) contributed to the elemental composition. Variability, evaluated as percent contribution of standard deviation to total elemental concentration, was greatest for cadmium (Cd) and molybdenum (Mo) at 4% and 3%, respectively. Peak values for the particle reactive micronutrients Cd and Mo, occurred in April and May, with a smaller enrichment in October (Fig. 6c). The spring and fall periods are also characterized by enrichment in total sterol concentration as discussed above. During the deployment period, net primary production for the months of April through June 2013 was 721, 698, and 775 g C m^{-2} d^{-1} respectively, whereas net primary production in the fall months of Sept. through Nov. 2012 was 372, 429, and 422 g C m^{-2} d^{-1} respectively (Fig. 6d). Hence, the spring phytoplankton bloom could have fueled the increase and export of fresh organic matter (e.g., phytodetritus) in the canyon during this season. The elevated pigment fluxes correspond to increased biomarker concentrations (especially sterols), indicating greater primary production and export of marine-derived organic matter. The simultaneous increase in the phytoplankton essential micronutrients of Cd and Mo during this period suggests increased scavenging, aggregation, and sinking of biomass during seasonal blooms in response to enhanced surface production within the nutricline (Wangersky *et al.*, 1989; Pohl *et al.*, 2004). The synchronous timing of the surface water primary productivity signal relative to the sediment trap geochemistry time series suggests rapid export and sinking of fresh particulate organic matter to the depositional zone of Baltimore Canyon. This corresponds to a spring maximum at the shelf break/slope waters (Ryan *et al.*, 1999; Xu *et al.*, 2011), and an increase in biomass on the MAB shelf during the spring and summer relative to the late fall (Mouw and Yoder, 2005).

Radiocarbon ages of sediment trap material recovered from the Baltimore Canyon deep lander site ranged between 980 (SD 15) and 1280 (SD 20) ^{14}C YBP with an average age of 1096 ^{14}C YBP (SD 18) (Table 5). The most negative $\Delta^{14}C$ value (-153.75‰) occurred in the first month of the deployment (September 2012), with little variability in $\Delta^{14}C$ ($\Delta\Delta^{14}C$ of 30‰) observed throughout the remaining part of the year. In comparison, fresh organic matter, as defined by coral tissue $\Delta^{14}C$ values,

469 was 30‰, consistent with surface water dissolved organic carbon $\Delta^{14}C$ values, ranging from 21 to
470 47‰. Therefore, the relatively "aged" material present in the trap suggests a mixture of marine and
471 terrestrial sources, as well as potential input from laterally advected refractory material (e.g., Druffel *et*
472 *al.*, 1986; Gordon and Goñi, 2003; Hwang and Druffel, 2003). The aged radiocarbon dates reflect
473 organic carbon that was photosynthetically fixed thousands of years ago, such as riverine carbon
474 exported from the Hudson River Watershed that has a $\Delta^{14}C$ signature of -350‰ (Raymond and Bauer,
475 2001). Fingerprinting and mixing approaches have been used in submarine canyons of the
476 Mediterranean Sea to identify relative source contributions (Tesi *et al.*, 2010; Pasqual *et al.*, 2013). In
477 our study, results of a two end-member $\Delta^{14}C$ mixing model yielded an annual average contribution
478 from terrestrial-derived carbon of ~48%, with the remaining ~52% attributed to autochthonous organic
479 matter produced from marine primary production. While selective degradation/preservation can alter
480 the source ^{14}C signature (Hwang *et al.*, 2010), results from the isotope mixing model are consistent
481 with annually averaged estimates based on molecular composition (Table 3).
482
483 Distal sources of terrestrial organic matter can be delivered via aeolian transport (Conte and Weber,
484 2002). However, surface sediment neodymium (Nd) isotope values from Baltimore Canyon and the
485 adjacent slope indicate that terrestrial sediment is primarily sourced from nearby riverine systems, such
486 as the Hudson River, where surface water moves southward, advecting riverine discharge towards
487 Baltimore Canyon and facilitating connectivity with adjacent watersheds (Ingham, 1992). Surface
488 sediments (0-0.5 cm) in the canyon were also enriched in terrestrial-derived sources of organic matter
489 relative to surface sediments on the slope (Supplementary Tables), demonstrating the accumulation of
490 terrestrial organic matter in the canyons relative to the slope. Transport of organic matter from
491 terrestrial sources is further facilitated by the presence of low-salinity, buoyant plume shelf waters on
492 the MAB (Churchill and Berger, 1998). This connectivity helps explain the terrestrial-derived organic
493 matter signature in the sediment trap samples and supports the hypothesis that submarine canyons
494 serve both as a conduit and reservoir of terrestrial organic matter to the deep sea (e.g., Tesi *et al.*,
495 2010).
496
497 *3.3 Canyon Zonation*
498 Substantial sedimentation/turbidity events prevented the collection of a complete time series for the
499 shallow and mid-depth sediment traps, precluding a comparison amongst the three deployments.
500 However, relative changes were detected for the period of overlap during the first two months
501 (September – October) that each trap was deployed. At the shallow site, mass fluxes were the greatest

and ^{210}Pb values were the lowest among the three trap sites (Table 1b), highlighting that resuspension dominates the shallow region. This is consistent with prior work demonstrating a zone of net convergence where internal tides travel up and down canyon, creating a region of elevated turbidity (Gardner, 1989a, b). Within this depth zone (~ 600 m), surface sediment samples consisted of coarse sand, small pebbles, and shell fragments at the sediment surface, presumably the result of local winnowing of the surface layer removing the fines. Bulk geochemical characteristics from the shallow and mid-depth traps were within the range observed at the deep site, indicating a mixture of marine and terrestrial derived matter throughout the canyon. This is represented by the trap material data from the shallow and mid-depth sites that plot along a mixing line, as reported above. Higher N:C ratios from the shallow-depth mooring site could suggest both greater proportion of marine-derived organic matter compared to the other sites and the dominance of fine-grained material in the deposition zones (Fig. 7b).

The relative molecular composition of the *n*-alkanes and sterols from the mid and shallow sites were similar to those reported for the deep site (Table 3). For example, *n*-C_{27} dominated the *n*-alkanes composition in the shallow and mid-depth trap sites, and cholesterol was the dominant sterol. However, the comparison between the three sediment traps also illustrates the accumulation and channeling of terrestrial organic matter farther down canyon with total *n*-alkane concentrations an order of magnitude greater at the deep site relative to the shallow and mid-depth sites, particularly the HMW *n*-alkanes (Table 2a). The hydrocarbons pristane and phytane were either below detection or at minimal concentrations at the shallow and mid-depth sites. Total sterol concentrations during the first two months were elevated at the shallow and mid-depth sites relative to the deep site, reflecting higher marine-sourced sterols exported from the nutricline (e.g., cholesterol and cholestanol). While limited in scope, the down canyon comparison captures spatial variability consistent with previously reported canyon depth zonation patterns. In addition, relative to surface samples (0-0.5 cm) from the canyon, surface samples from the adjacent slope yield lower terrestrial contribution, and an anthropogenic component was absent from the slope surface sediment samples (Supplementary Table S4), supporting the notion that canyons may serve as a conduit of terrestrial organic matter and contaminants. These observations reflect the interplay of hydrodynamics and geomorphology, which channel and concentrate sediment and organic matter within the canyon, leading to differences in organic matter composition in Baltimore Canyon.

4. Summary

By examining a unique set of geochemical variables, this study demonstrated the relationship between particulate matter composition in the context of seasonal variation in surface water biological production and export through the nutricline in Baltimore Canyon. The sediment trap biomarker compositions, together with bulk characteristics, indicate that both terrestrial OM and marine derived OM are important food sources, suggesting that both vertical and lateral transport across the continental margin are important processes to the deposition zone of Baltimore Canyon. However, details in the temporal variability of the OM provenance reveal a larger contribution from marine-derived OM in the spring, which is characterized by increased scavenging, aggregation, and sinking of fresh, recently exported OM from the upper water column during a spring bloom. Connectivity to adjacent watershed also facilitates offshore transport of "aged" terrestrial organic matter and nutrients. Results presented here demonstrate how OM content and OM provenance signature can be linked to seasonal events (e.g., surface productivity blooms), episodic events (e.g., resuspension), as well as those processes occurring permanent, such as the presence of the nepheloid layer. Therefore, variability is a key feature influencing the deep-sea food web, with faunal composition and carbon cycling influenced by seasonal or episodic fluxes in particulate matter composition. Such deposition patterns in turn may be the greatest contributors to canyons exhibiting biodiversity and productivity maxima. With the majority of deep-sea canyons being poorly sampled, results presented here suggest that the submarine canyons of the MAB region are a key contributor to global estimates of benthic biomass and productivity in the deep sea by serving as conduits for transport of terrestrial and marine derived organic matter.

5. Acknowledgements

The authors thank the Bureau of Ocean Energy Management (BOEM), USGS, and the National Oceanic and Atmospheric Administration (NOAA) Office of Ocean Exploration and Research for major funding and ship support. We also thank the DISCOVRE Mid-Atlantic Canyons project and the crews of the NOAA ships *Nancy Foster* and *Ronald H. Brown*, J. Borden, O. Cheriton, and K. Rosenberger (USGS). Funding was provided to N. Prouty from the USGS Environments Program through the Outer Continental shelf study DISCOVRE Mid-Atlantic Canyons. F. Mienis is financially supported by the Innovational Research Incentives Scheme of the Netherlands Organisation for Scientific Research (NWO-VIDI). Any use of trade, product, or firm names is for descriptive purposes only and does not imply endorsement by the U.S. Government. Comments from two anonymous reviewers greatly improved the manuscript.

Figures

Figure 1

Multibeam bathymetry of Baltimore Canyon showing position of benthic landers (white plus sign) and mooring (white star) at the shallow (a), mid (b) and deep (c) sites. Progressive vector plots show the

cumulative movement of water at shallow (a), mid (b) and deep (c) sites, split into 60 day subsets (black lines indicating Sept-Nov, green Nov-Jan, grey Jan-Mar, red Mar-May). Grey line and circles (i) show the individual CTD casts that make up the transect along the axis of the canyon (two stations were used for water sampling, ii=NF-2012-036 and iii=NF-2012-040) as shown in Figure 3. Black triangles represent CTD casts used for water and trace element sampling (iv=NF-2012-138, v=NF-2012-128, vi=NF-2012-051, vii=NF-2012-130, viii=NF-2012-149, ix=NF-2012-073). Note some stations are shown with an offset line for clarity. Inset figure shows the location of Baltimore Canyon (black box) with respect to the Mid-Atlantic Bight and neighboring states of Maryland (MD), Virginia (VA) and Delaware (DE). Contour lines show depth in meters.

Figure 2

Oceanographic variables (y-axis) recorded by the shallow lander (603 m), mid-mooring (1082 m, note no turbidity sensor) and deep lander (1318 m) in Baltimore Canyon. Black or white lines represent a 24-hour moving average. For the shallow and deep landers all sensors recorded at 1.5 m above bottom except for currents at 2 m above bottom, which were recorded at a 15 min interval. For the mid-mooring, current data was obtained at 14 m above bottom and temperature at 9 m above bottom. Currents were recorded at a 15-minute interval. Temperature was recorded at a 5-minute interval and was resampled to a 15-minute interval to match other sensors.

Figure 3

Baltimore Canyon nepheloid layer distribution along the canyon axis, derived from CTD profiles with overlaid isopycnals (kg m^{-3}). Vertical lines show the position of CTD casts along the transect, including extreme margins in the plot (number of casts = 9). Turbidity expressed as relative Formazin turbidity units (FTU).

Figure 4

Trace element concentrations (μg g^{-1}; neodymium [Nd], lanthanium [La], aluminum [Al], and iron [Fe]) in suspended particulate matter filtered (>0.45 μm) at discrete water column depths from CTD casts in Baltimore Canyon and adjacent slope. Gray bar indicates zones of elevated turbidity derived from CTD casts.

Figure 5

Nutrient vertical depth profiles from Baltimore Canyon sampled in 2012 along a down-canyon transect for (a) nitrate, (b) phosphate, and (c) silicate (μmol L^{-1}) at four CTD stations, including NF12-036, NF12-040, N12-051, and NF12-073. Dissolved oxygen (black line) derived from the CTD sensor is shown for the Baltimore Canyon deep station (NF-12-040). Gray bar indicates depth of nutricline defined from nutrient profiles collected during the August 2012 sampling cruise. (d) Down canyon temperature (°C) profile derived from CTD casts.

Figure 6

Time-series for bulk sediment measurements and molecular biomarker composition derived from ~monthly sediment trap samples deployed from September 5, 2012 to June 23, 2013. Results are shown for (a) mass flux (g m^{-2} d^{-1}) and ^{210}Pb (mBq g^{-1}), (b) total sterol and *n*-alkane concentration (μg g^{-1} C) and chlorophyll-*a* (mg g^{-1}), (c) cadmium (Cd) and molybdenum (Mo) (μg g^{-1}), and (d) net primary production (g C m^{-2} d^{-1}; http://www.science.oregonstate.edu/ocean.productivity/index.php).

Figure 7

(a) Stable isotope composition of carbon ($\delta^{13}C$; ‰) versus total nitrogen:organic carbon (N:C) ratio from the deep sediment trap (1318 m) samples. The potential sources of organic carbon (C3 vascular plants, C3 soil organic matter, heterotrophic bacteria, and marine phytoplankton) are shown to highlight mixed sources of organic matter to the deep-sea sediment samples. The N:C ratio is plotted versus $\delta^{13}C$ rather than the C:N ratio because the N:C ratio behaves linearly in a mixing model (Goñi *et al.*, 2003). (b) Results from the shallow (603 m) and mid-depth (1082) sites relative to the deep site for the months of overlap (Aug-Sept. 2012).

References:

Armstrong, F.A.J., Stearns, C.R., Strickland, J.D.H., 1967. The measurement of upwelling and subsequent biological process by means of the Technicon Autoanalyzer® and associated equipment. Elsevier, pp. 381-389.

Behrenfeld, M.J., Falkowski, P.G., 1997. Photosynthetic rates derived from satellite-based chlorophyll concentration. Limnology and Oceanography 42 (1), 1-20.

Bernhardt, H., Wilhelms, A., 1967. The continuous determination of low level iron, soluble phosphate and total phosphate with the AutoAnalyzer. pp. 385-389.

Bianchi, T.S., Canuel, E.A., 2011. Chemical biomarkers in aquatic ecosystems. Princeton University Press. 329 pp.

Blumer, M., Mullin, M.M., Thomas, D.W., 1963. Pristane in zooplankton. Science 140, 974-974.

Bray, E.E., Evans, E.D., 1961. Distribution of n-paraffins as a clue to recognition of source beds.

640 Boer, W., van den Bergh, G.D., de Haas, H., de Stigter, H.C., Gieles, R., van Weering, T.C.E., 2006.
641 Validation of accumulation rates in Teluk Banten (Indonesia) from commonly applied ^{210}Pb
642 models, using the 1883 Krakatau tephra as time marker. Marine Geology 227 (3–4), 263-277.
643 Geochimica et Cosmochimica Acta 22 (1), 2-15.
644 Briggs, P.H., Meier, A.L., 2002. The determination of forty-two elements in geological materials by
645 inductively coupled plasma – mass spectrometry. USGS Open File Report 02-223-I.
646 Brooke, S., Ross, S.W., 2014. First observations of the cold-water coral Lophelia pertusa in mid-
647 Atlantic canyons of the USA. Deep Sea Research Part II: Topical Studies in Oceanography 104,
648 245-251.
649 Brooke, S.D., Watts, M.W., Heil, A.D., Rhode, M., Mienis, F., Duineveld, G.C.A., Davies, A.J., Ross,
650 S.W., 2016. Distributions and habitat associations of deep-water corals in Norfolk and Baltimore
651 Canyons, Mid-Atlantic Bight, USA. Deep Sea Research Part II: Topical Studies in Oceanography.
652 Canals, M., Puig, P., Durrieu de Madron, X., Heussner, S., Palanques, A., Fabres, J., 2006. Flushing
653 submarine canyons. Nature 444 (7117), 354-357.
654 Carney, R., Gibson, R., Atkinson, R., Gordon, J., 2005. Zonation of deep biota on continental margins.
655 Oceanography and Marine Biology Annual Review 43, 211-278.
656 Choi, B.-J., Wilkin, J.L., 2007. The effect of wind on the dispersal of the Hudson River Plume. Journal
657 of Physical Oceanography 37 (7), 1878-1897.
658 Churchill, J.H., Berger, T.J., 1998. Transport of middle Atlantic Bight shelf water to the Gulf Stream
659 near Cape Hatteras. Journal of Geophysical Research: Oceans 103 (C13), 30605-30621.
660 Conte, M.H., Weber, J.C., 2002. Plant biomarkers in aerosols record isotopic discrimination of
661 terrestrial photosynthesis. Nature 417 (6889), 639-641.
662 Costa, A.M., Mil-Homens, M., Lebreiro, S.M., Richter, T.O., de Stigter, H., Boer, W., Trancoso, M.A.,
663 Melo, Z., Mouro, F., Mateus, M., 2011. Origin and transport of trace metals deposited in the
664 canyons off Lisboa and adjacent slopes (Portuguese Margin) in the last century. Marine Geology
665 282 (3), 169-177.
666 De Leo, F.C., Smith, C.R., Rowden, A.A., Bowden, D.A., Clark, M.R., 2010. Submarine canyons:
667 hotspots of benthic biomass and productivity in the deep sea. Proceedings of the Royal Society of
668 London B: Biological Sciences.
669 DeMaster, D.J., Pope, R.H., Levin, L.A., Blair, N.E., 1994. Biological mixing intensity and rates of
670 organic carbon accumulation in North Carolina slope sediments. Deep Sea Research Part II:
671 Topical Studies in Oceanography 41 (4), 735-753.
672 Druffel, E.R.M., Honju, S., Griffin, S., Wong, C., 1986. Radiocarbon in particulate matter from the
673 eastern sub-arctic Pacific Ocean; evidence of a source of terrestrial carbon to the deep sea.
674 Radiocarbon 28 (2A), 397-407.
675 Duineveld, G., Lavaleye, M., Berghuis, E., De Wilde, P., 2001. Activity and composition of the
676 benthic fauna in the Whittard Canyon and the adjacent continental slope (NE Atlantic).
677 Oceanologica Acta 24 (1), 69-83.
678 Eglinton, T.I., Eglinton, G., 2008. Molecular proxies for paleoclimatology. Earth and Planetary
679 Science Letters 275 (1), 1-16.
680 Ficken, K.J., Li, B., Swain, D.L., Eglinton, G., 2000. An *n*-alkane proxy for the sedimentary input of
681 submerged/floating freshwater aquatic macrophytes. Organic Geochemistry 31 (7–8), 745-749.
682 Garcia, R., Koho, K.A., De Stigter, H.C., Epping, E., Koning, E., Thomsen, L., 2007. Distribution of
683 meiobenthos in the Nazare canyon and adjacent slope (western Iberian Margin) in relation to
684 sedimentary composition. Marine Ecology Progress Series 340, 207-220.
685 Gardner, W.D., 1989a. Baltimore Canyon as a modern conduit of sediment to the deep sea. Deep Sea
686 Research Part A. Oceanographic Research Papers 36 (3), 323-358.
687 Gardner, W.D., 1989b. Periodic resuspension in Baltimore Canyon by focusing of internal waves.
688 Journal of Geophysical Research: Oceans 94 (C12), 18185-18194.

689 Gardner, W.D., Tucholke, B.E., Richardson, M.J., Biscaye, P.E., 2017. Benthic storms, nepheloid
690 layers, and linkage with upper ocean dynamics in the western North Atlantic. Marine Geology 385,
691 304-327.
692 Gibson, R.N., Atkinson, R.J.A., Gordon, J.D.M., 2005. Zonation of deep biota on continental margins.
693 Oceanography and Marine Biology: An Annual Review 43, 211-278.
694 Goni, M.A., Ruttenberg, K.C., Eglinton, T.I., 1997. Sources and contribution of terrigenous organic
695 carbon to surface sediments in the Gulf of Mexico. Nature 389 (6648), 275-278.
696 Goñi, M.A., Teixeira, M.J., Perkey, D.W., 2003. Sources and distribution of organic matter in a river-
697 dominated estuary (Winyah Bay, SC, USA). Estuarine, Coastal and Shelf Science 57 (5), 1023-
698 1048.
699 Gooday, A.J., 2002. Biological responses to seasonally varying fluxes of organic matter to the ocean
700 floor: a review. Journal of Oceanography 58 (2), 305-332.
701 Gordon, E.S., Goñi, M.A., 2003. Sources and distribution of terrigenous organic matter delivered by
702 the Atchafalaya River to sediments in the northern Gulf of Mexico. Geochimica et Cosmochimica
703 Acta 67 (13), 2359-2375.
704 Harwood, J.E., Kühn, A.L., 1970. A colorimetric method for ammonia in natural waters. Water
705 Research 4 (12), 805-811.
706 Hecker, B., 1980. Scleractinians (stony corals) encountered in this study: Appendix C. Canyon
707 Assessment Study no. BLM-AA551-CT8-49. U.S. Department of Interior, Bureau of Land
708 Management, Washington, DC.
709 Hecker, B., Logan, D.T., Gandarillas, F.E., Gibson, P.R., 1983. Megafaunal assemblages in Lydonia
710 Canyon, Baltimore Canyon, and selected slope areas. Canyon and Slope Processes Study, Final
711 Report prepared for the U.S. Department of the Interior. Minerals Management Service,
712 Washington, D.C. .
713 Hedges, J.I., Parker, P.L., 1976. Land-derived organic matter in surface sediments from the Gulf of
714 Mexico. Geochimica et Cosmochimica Acta 40 (9), 1019-1029.
715 Howatt, T.M., Allen, S.E., 2013. Impact of the continental shelf slope on upwelling through submarine
716 canyons. Journal of Geophysical Research: Oceans 118 (10), 5814-5828.
717 Hunter, W.R., Jamieson, A., Huvenne, V.A.I., Witte, U., 2013. Sediment community responses to
718 marine vs. terrigenous organic matter in a submarine canyon. Biogeosciences 10, 67-80.
719 Hwang, J., Druffel, E.R.M., 2003. Lipid-like material as the source of the uncharacterized organic
720 carbon in the ocean? Science 299 (5608), 881-884.
721 Hwang, J., Druffel, E.R.M., Eglinton, T.I., 2010. Widespread influence of resuspended sediments on
722 oceanic particulate organic carbon: Insights from radiocarbon and aluminum contents in sinking
723 particles. Global Biogeochemical Cycles 24 (4).
724 Ingham, M.C., 1992. Summary of the physical oceanographic processes and features pertinent to
725 pollution distribution in the coastal and offshore waters of the northeastern United States, Virginia
726 to Maine. In: Ingham, M.C. (Ed.), NOAA Technical Memorandum NMFS-FNEC-17. National
727 Oceanic and Atmospheric Administration, Woods Hole, MA.
728 Knauer, G.A., Asper, V., 1989. Sediment trap technology and sampling, Report of the US JGOFS
729 working group on sediment trap technology and sampling, University of South Mississippi, USA,
730 14–16 November 1988, US JGOFS Planning report No 10, WHOI, August 1989, 94pp.
731 Lee, C., Hedges, J.I., Wakeham, S.G., Zhu, N., 1992. Effectiveness of various treatments in retarding
732 microbial activity in sediment trap material and their effects on the collection of swimmers.
733 Limnology and Oceanography 37 (1), 117-130.
734 Levin, L.A., Etter, R.J., Rex, M.A., Gooday, A.J., Smith, C.R., Pineda, J., Stuart, C.T., Hessler, R.R.,
735 Pawson, D., 2001. Environmental Influences on Regional Deep-Sea Species Diversity 1. Annual
736 Review of Ecology and Systematics 32 (1), 51-93.

737 Levin, L.A., Sibuet, M., 2012. Understanding continental margin biodiversity: a new imperative.
738 Annual Review of Marine Science 4, 79-112.
739 Martín, J., Palanques, A., Vitorino, J., Oliveira, A., De Stigter, H.C., 2011. Near-bottom particulate
740 matter dynamics in the Nazaré submarine canyon under calm and stormy conditions. Deep Sea
741 Research Part II: Topical Studies in Oceanography 58 (23), 2388-2400.
742 Meyers, P.A., 1994. Preservation of elemental and isotopic source identification of sedimentary
743 organic matter. Chemical Geology 114 (3–4), 289-302.
744 Mouw, C.B., Yoder, J.A., 2005. Primary production calculations in the Mid-Atlantic Bight, including
745 effects of phytoplankton community size structure. Limnology and Oceanography 50 (4), 1232-
746 1243.
747 Obelcz, J., Brothers, D., Chaytor, J., Brink, U.t., Ross, S.W., Brooke, S., 2014. Geomorphic
748 characterization of four shelf-sourced submarine canyons along the U.S. Mid-Atlantic continental
749 margin. Deep Sea Research Part II: Topical Studies in Oceanography 104, 106-119.
750 Oczkowski, A., Kreakie, B., McKinney, R.A., Prezioso, J., 2016. Patterns in stable isotope values of
751 nitrogen and carbon in particulate matter from the Northwest Atlantic Continental Shelf, from the
752 Gulf of Maine to Cape Hatteras. Frontiers in Marine Science 3 (252), 1-9.
753 Palanques, A., Durrieu de Madron, X., Puig, P., Fabres, J., Guillén, J., Calafat, A., Canals, M.,
754 Heussner, S., Bonnin, J., 2006. Suspended sediment fluxes and transport processes in the Gulf of
755 Lions submarine canyons. The role of storms and dense water cascading. Marine Geology 234 (1),
756 43-61.
757 Pasqual, C., Goñi, M.A., Tesi, T., Sanchez-Vidal, A., Calafat, A., Canals, M., 2013. Composition and
758 provenance of terrigenous organic matter transported along submarine canyons in the Gulf of Lion
759 (NW Mediterranean Sea). Progress in Oceanography 118, 81-94.
760 Pisani, O., Oros, D.R., Oyo-Ita, O.E., Ekpo, B.O., Jaffé, R., Simoneit, B.R.T., 2013. Biomarkers in
761 surface sediments from the Cross River and estuary system, SE Nigeria: Assessment of organic
762 matter sources of natural and anthropogenic origins. Applied Geochemistry 31 (0), 239-250.
763 Planquette, H., Sherrell, R.M., 2012. Sampling for particulate trace element determination using water
764 sampling bottles: methodology and comparison to in situ pumps. Limnology and Oceanography:
765 Methods 10 (5), 367-388.
766 Pohl, C., Löffler, A., Hennings, U., 2004. A sediment trap flux study for trace metals under seasonal
767 aspects in the stratified Baltic Sea (Gotland Basin; 57 19.20′ N; 20 03.00′ E). Marine Chemistry 84
768 (3), 143-160.
769 Prahl, F.G., Bennett, J.T., Carpenter, R., 1980. The early diagenesis of aliphatic hydrocarbons and
770 organic matter in sedimentary particulates from Dabob Bay, Washington. Geochimica et
771 Cosmochimica Acta 44 (12), 1967-1976.
772 Prouty, N.G., Campbell, P.L., Mienis, F., Duineveld, G., Demopoulos, A.W.J., Ross, S.W., Brooke, S.,
773 2016. Impact of Deepwater Horizon spill on food supply to deep-sea benthos communities.
774 Estuarine, Coastal and Shelf Science 169, 248-264.
775 Puig, P., Canals, M., Company, J.B., Martín, J., Amblas, D., Lastras, G., Palanques, A., Calafat, A.M.,
776 2012. Ploughing the deep sea floor. Nature 489 (7415), 286-289.
777 Puig, P., Palanques, A., Martín, J., 2014. Contemporary sediment-transport processes in submarine
778 canyons. Annual Review of Marine Science 6, 53-77.
779 Pusceddu, A., Dell'Anno, A., Fabiano, M., Danovaro, R., 2009. Quantity and bioavailability of
780 sediment organic matter as signatures of benthic trophic status. Marine Ecology Progress Series
781 375, 41-52.
782 Raymond, P.A., Bauer, J.E., 2001. Use of ^{14}C and ^{14}C natural abundances for evaluating riverine,
783 estuarine, and coastal DOC and POC sources and cycling: a review and synthesis. Organic
784 Geochemistry 32 (4), 469-485.

785 Rex, M.A., Etter, R.J., 2010. Deep-sea Biodiversity: Pattern and Scale. Harvard University Press,
786 Print, Cambridge. 354 pp.
787 Romero-Romero, S., Molina-Ramírez, A., Höfer, J., Duineveld, G., Rumín-Caparrós, A., Sanchez-
788 Vidal, A., Canals, M., Acuña, J.L., 2016. Seasonal pathways of organic matter within the Avilés
789 submarine canyon: Food web implications. Deep Sea Research Part I: Oceanographic Research
790 Papers 117, 1-10.
791 Ryan, J.P., Yoder, J.A., Cornillon, P.C., 1999. Enhanced chlorophyll at the shelfbreak of the Mid-
792 Atlantic Bight and Georges Bank during the spring transition. Limnology and Oceanography 44
793 (1), 1-11.
794 Schaff, T., Levin, L., Blair, N., DeMaster, D., Pope, R., Boehme, S., 1992. Spatial heterogeneity of
795 benthos on the Carolina continental slope: large (100 km)-scale variation. Marine Ecology-
796 Progress Series 88, 143-143.
797 Schlitzer, R., 2016. Ocean Data View. http://odv.awi.de.
798 Soltwedel, T., 2000. Metazoan meiobenthos along continental margins: a review. Progress in
799 Oceanography 46 (1), 59-84.
800 Stuiver, M., Polach, H.A., 1977. Discussion reporting of 14C data. Radiocarbon 19 (3), 355-363.
801 Tesi, T., Miserocchi, S., Goñi, M.A., Langone, L., 2007. Source, transport and fate of terrestrial
802 organic carbon on the western Mediterranean Sea, Gulf of Lions, France. Marine Chemistry 105
803 (1), 101-117.
804 Tesi, T., Puig, P., Palanques, A., Goñi, M.A., 2010. Lateral advection of organic matter in cascading-
805 dominated submarine canyons. Progress in Oceanography 84 (3), 185-203.
806 Tolosa, I., Miquel, J.C., Gasser, B., Raimbault, P., Goyet, C., Claustre, H., 2008. Distribution of lipid
807 biomarkers and carbon isotope fractionation in contrasting trophic environments of the South East
808 Pacific. Biogeosciences 5 (3), 949-968.
809 Vetter, E.W., Dayton, P.K., 1998. Macrofaunal communities within and adjacent to a detritus-rich
810 submarine canyon system. Deep Sea Research Part II: Topical Studies in Oceanography 45 (1), 25-
811 54.
812 Vogel, J.S., Southon, J.R., Nelson, D.E., 1987. Catalyst and binder effects in the use of filamentous
813 graphite for AMS. Nuclear Instruments & Methods in Physics Research Section B-Beam
814 Interactions with Materials and Atoms 29 (1-2), 50-56.
815 Volkman, J.K., 1986. A review of sterol markers for marine and terrigenous organic matter. Organic
816 Geochemistry 9, 83-99.
817 Volkman, J.K., Revill, A.T., Holdsworth, D.G., Fredericks, D., 2008. Organic matter sources in an
818 enclosed coastal inlet assessed using lipid biomarkers and stable isotopes. Organic Geochemistry
819 39 (6), 689-710.
820 Wakeham, S.G., Lee, C., Hedges, J.I., Hernes, P.J., Peterson, M.J., 1997. Molecular indicators of
821 diagenetic status in marine organic matter. Geochimica et Cosmochimica Acta 61 (24), 5363-5369.
822 Wakeham, S.G., Canuel, E.A., 2006. Degradation and preservation of organic matter in marine
823 sediments. In: K., V.J. (Ed.), The Handbook of Environmental Chemistry, Reactions and
824 Processes. Part N: Marine Organic Matter: Biomarkers, Isotopes and DNA. Springer-Verlag,
825 Berlin, pp. 295-321.
826 Wakeham, S.G., McNichol, A.P., 2014. Transfer of organic carbon through marine water columns to
827 sediments - insights from stable and radiocarbon isotopes of lipid biomarkers. Biogeosciences 11
828 (23), 6895-6914.
829 Wangersky, P.J., Moran, S.B., Pett, R.J., Slauernwhite, D.E., Zhou, X., 1989. Biological control of
830 trace metal residence times: an experimental approach. Marine Chemistry 28 (1-3), 215-226.
831 Wei, C.-L., Rowe, G.T., Hubbard, G.F., Scheltema, A.H., Wilson, G.D.F., Petrescu, I., Foster, J.M.,
832 Wicksten, M.K., Chen, M., Davenport, R., 2010. Bathymetric zonation of deep-sea macrofauna in
833 relation to export of surface phytoplankton production. Marine Ecology Progress Series 399, 1-14.

834 Witbaard, R., Duineveld, G.C.A., Van der Weele, J.A., Berghuis, E.M., Reyss, J.P., 2000. The benthic
835 response to the seasonal deposition of phytopigments at the Porcupine Abyssal Plain in the North
836 East Atlantic. Journal of Sea Research 43 (1), 15-31.
837 Xu, Y., Chant, R., Gong, D., Castelao, R., Glenn, S., Schofield, O., 2011. Seasonal variability of
838 chlorophyll a in the Mid-Atlantic Bight. Continental Shelf Research 31 (16), 1640-1650.
839

Figure 1

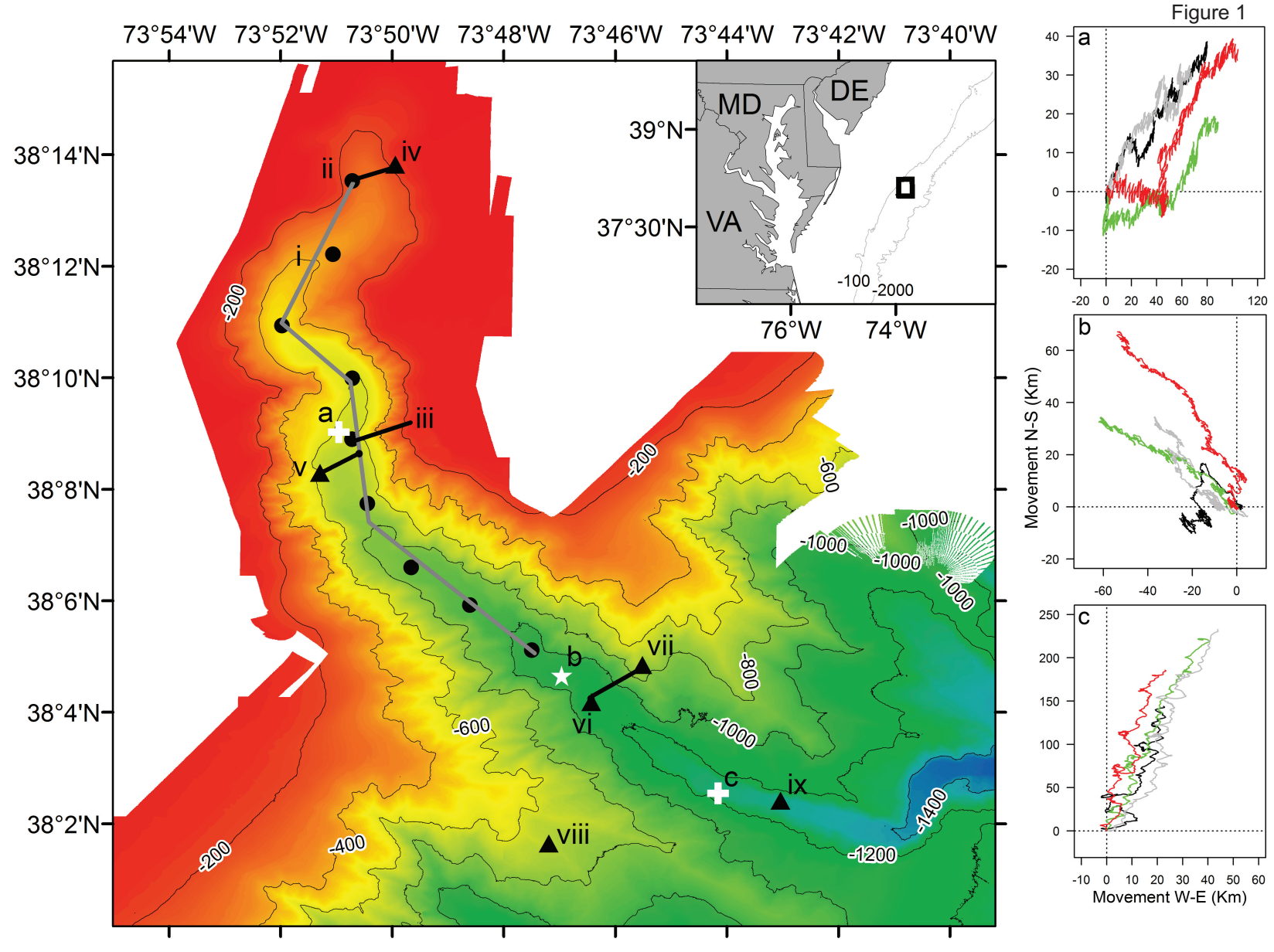
73°54'W
73°52'W
73°50'W
73°48'W
73°46'W
73°44'W
73°42'W
73°40'W
38°14'N
38°12'N
38°10'N
38°8'N
38°6'N
38°4'N
38°2'N
MD
DE
VA
39°N
37°30'N
76°W
74°W
-100
-2000
-200
-400
-600
-800
-1000
-1200
-1400
i
ii
iii
iv
v
vi
vii
viii
ix
a
b
c
a
b
c
Movement N-S (Km)
Movement W-E (Km)

Figure 2

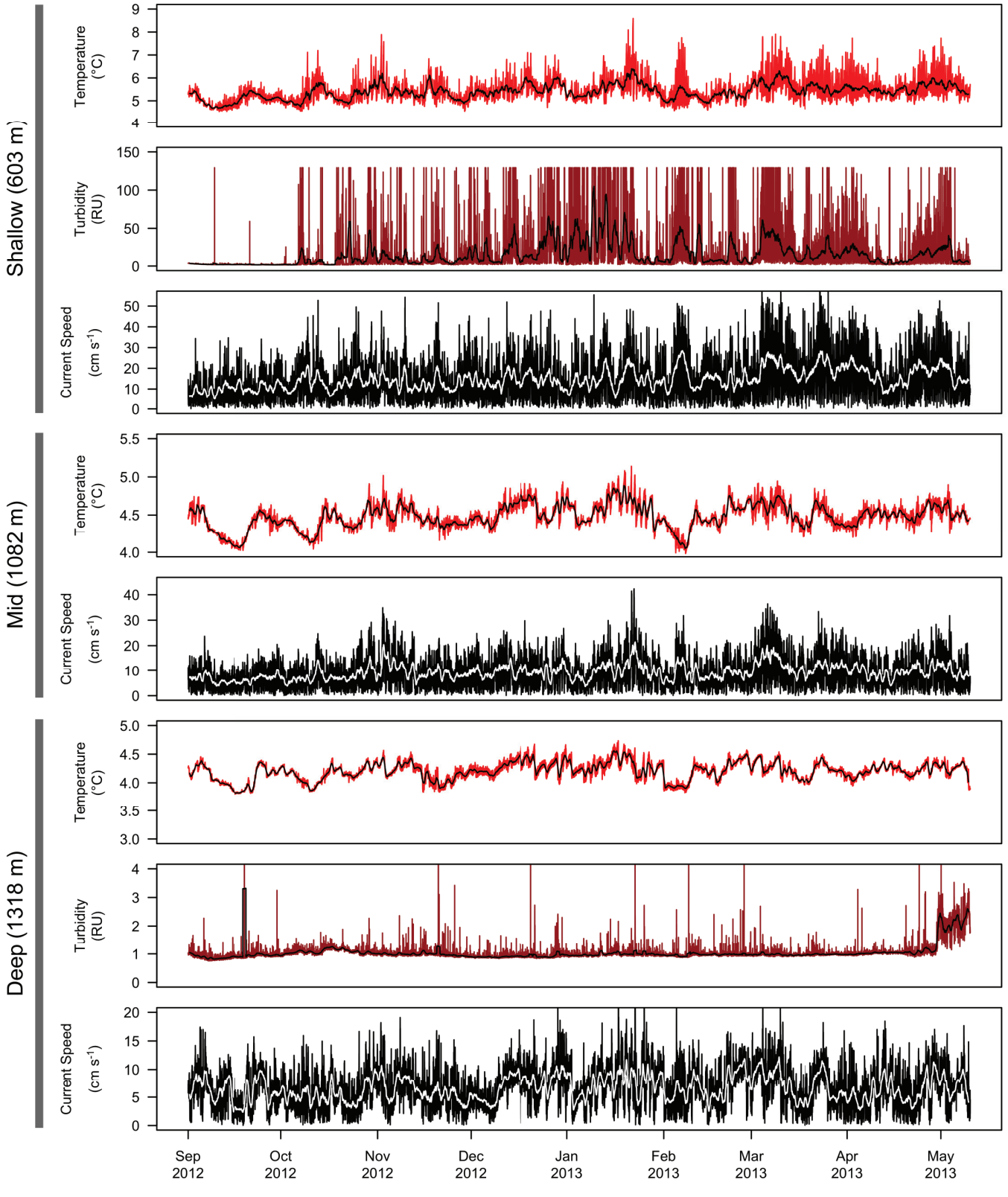
Shallow (603 m)
Temperature (°C)
Turbidity (RU)
Current Speed (cm s-1)
Mid (1082 m)
Temperature (°C)
Current Speed (cm s-1)
Deep (1318 m)
Temperature (°C)
Turbidity (RU)
Current Speed (cm s-1)
Sep 2012
Oct 2012
Nov 2012
Dec 2012
Jan 2013
Feb 2013
Mar 2013
Apr 2013
May 2013

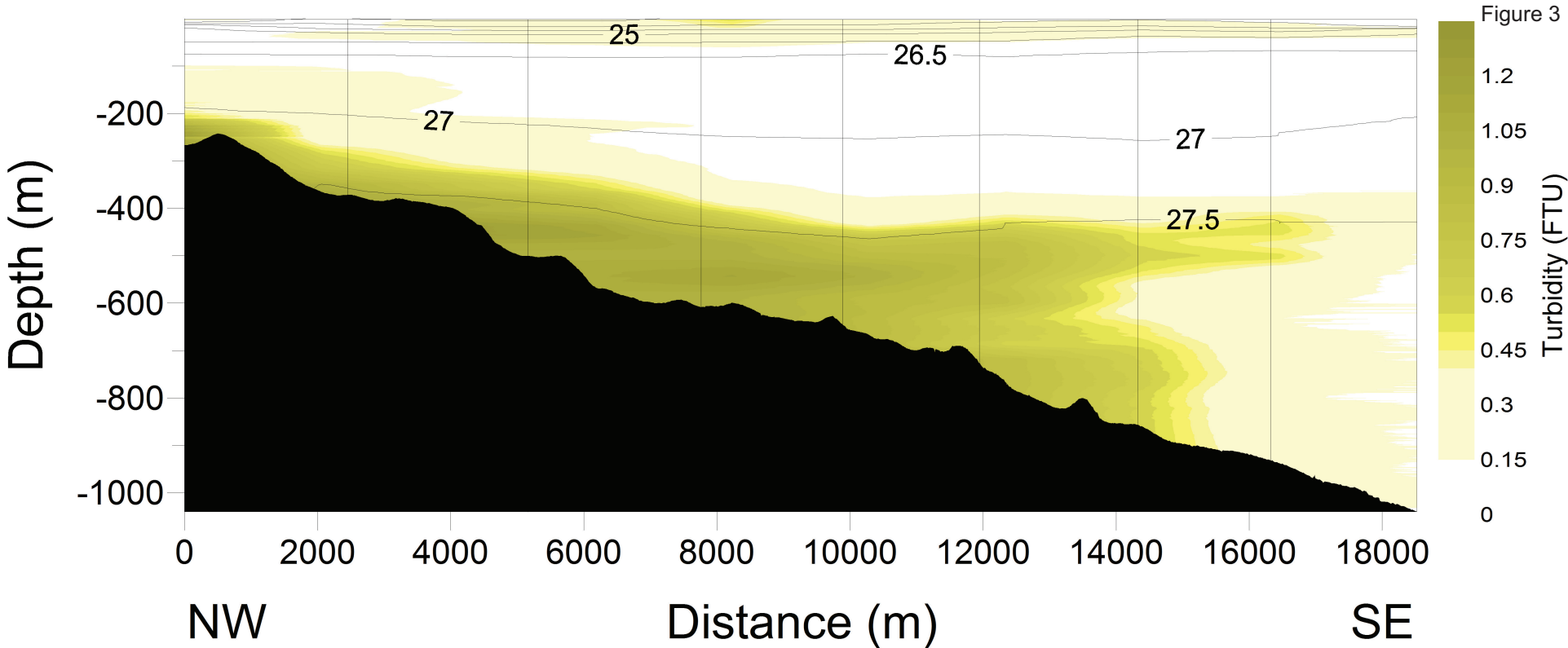
Figure 3
25
26.5
27
27
27.5
-200
-400
-600
-800
-1000
Depth (m)
0
2000
4000
6000
8000
10000
12000
14000
16000
18000
NW
Distance (m)
SE
1.2
1.05
0.9
0.75
0.6
0.45
0.3
0.15
0
Turbidity (FTU)

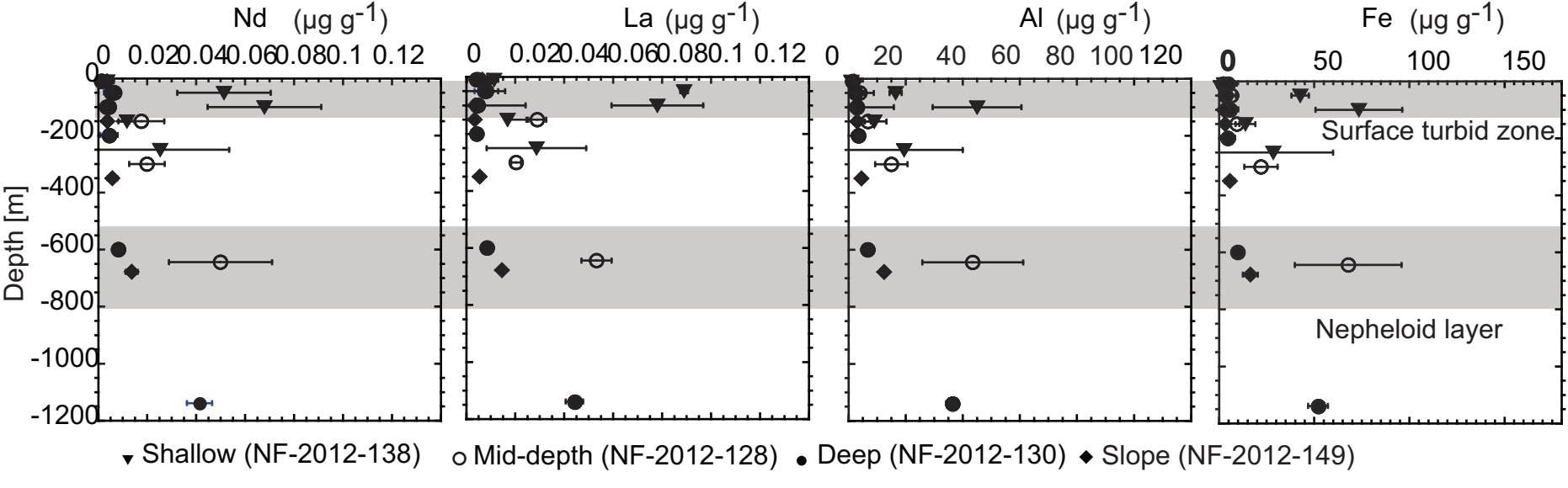
Nd (μg g-1)
La (μg g-1)
Al (μg g-1)
Fe (μg g-1)
0 0.02 0.04 0.06 0.08 0.1 0.12
0 20 40 60 80 100 120
0 50 100 150
Depth [m]
0
-200
-400
-600
-800
-1000
-1200
Surface turbid zone
Nepheloid layer
Shallow (NF-2012-138)
Mid-depth (NF-2012-128)
Deep (NF-2012-130)
Slope (NF-2012-149)

Figure 5

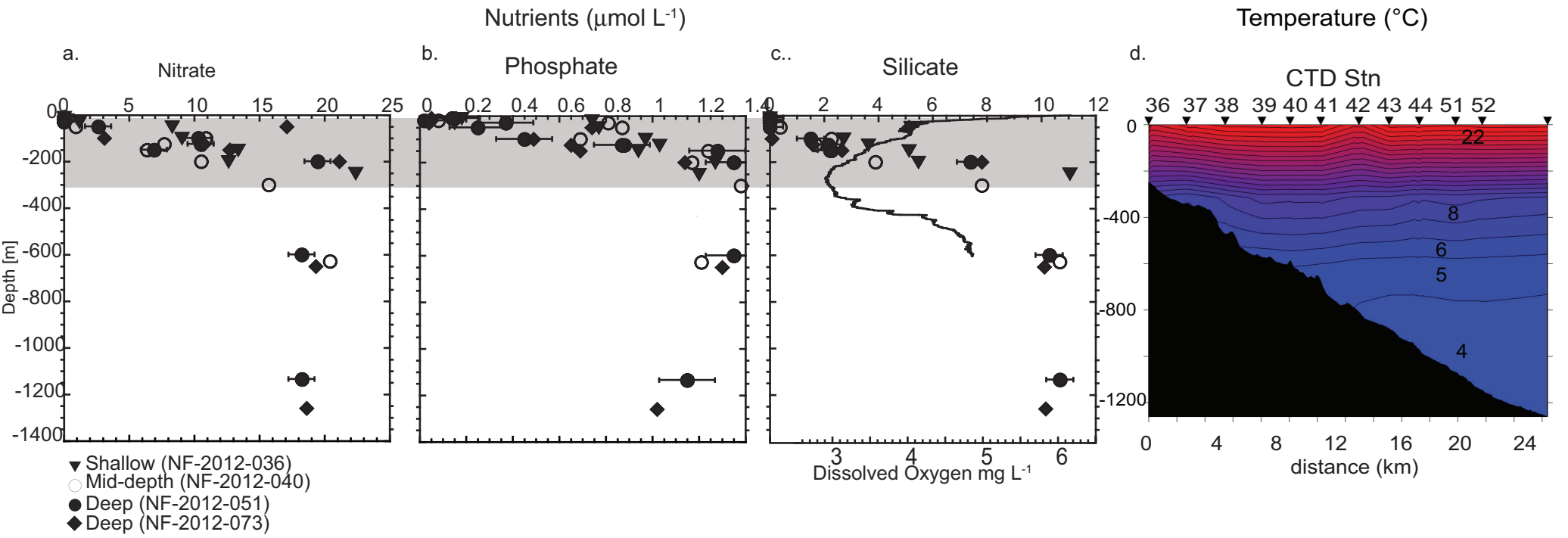
Nutrients (µmol L-1)
a.
Nitrate
b.
Phosphate
c..
Silicate
d.
Temperature (°C)
CTD Stn
36 37 38 39 40 41 42 43 44 51 52
Depth [m]
0
-200
-400
-600
-800
-1000
-1200
-1400
0 5 10 15 20 25
0 0.2 0.4 0.6 0.8 1 1.2 1.4
0 2 4 6 8 10 12
3 4 5 6
Dissolved Oxygen mg L-1
22
8
6
5
4
0 4 8 12 16 20 24
distance (km)
▼ Shallow (NF-2012-036)
○ Mid-depth (NF-2012-040)
● Deep (NF-2012-051)
◆ Deep (NF-2012-073)

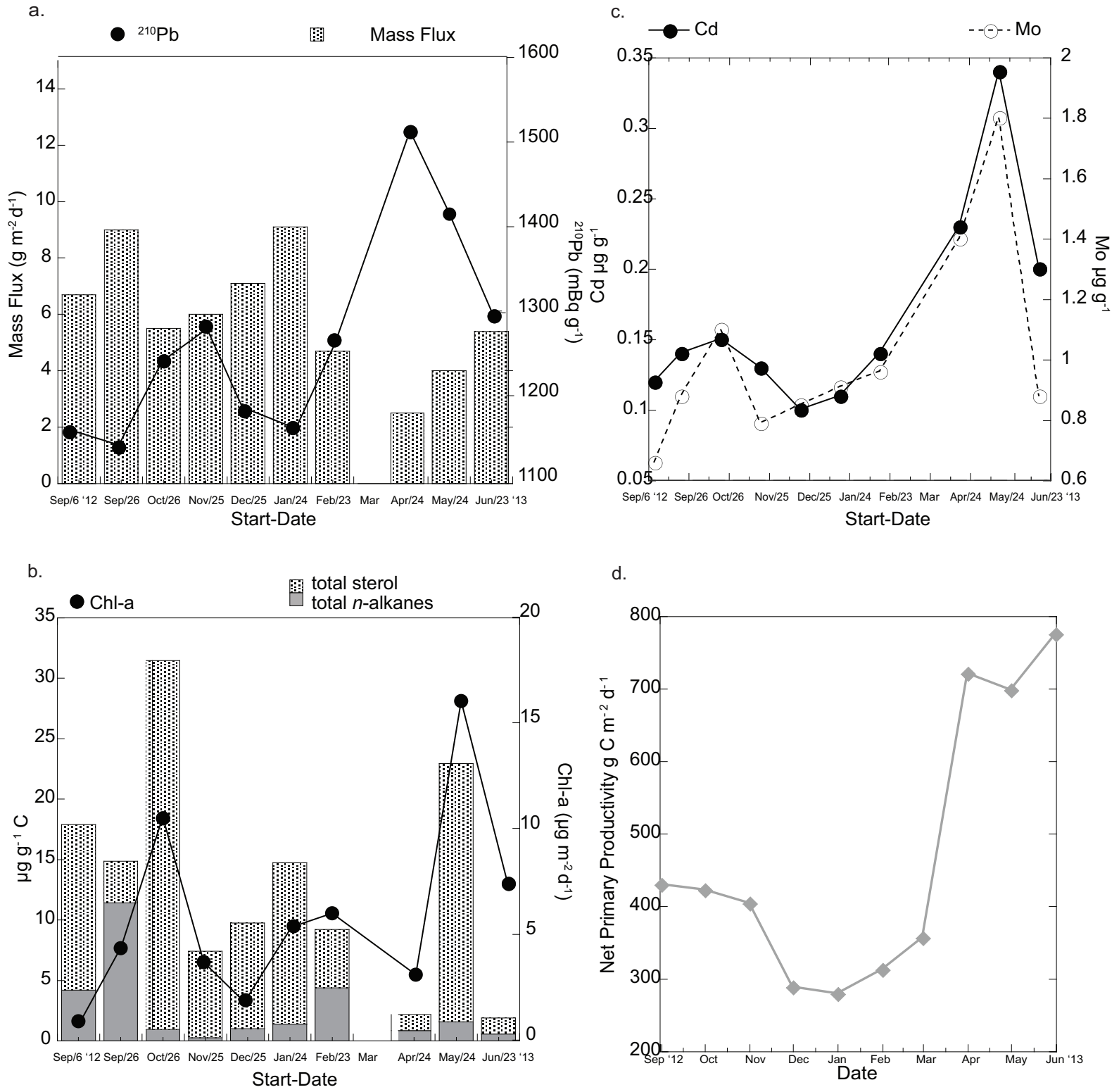
a.
^{210}Pb
Mass Flux
Mass Flux (g m^{-2} d^{-1})
^{210}Pb (mBq g^{-1})
Sep/6 '12 Sep/26 Oct/26 Nov/25 Dec/25 Jan/24 Feb/23 Mar Apr/24 May/24 Jun/23 '13
Start-Date
c.
Cd
Mo
Cd µg g^{-1}
Mo µg g^{-1}
Sep/6 '12 Sep/26 Oct/26 Nov/25 Dec/25 Jan/24 Feb/23 Mar Apr/24 May/24 Jun/23 '13
Start-Date
b.
Chl-a
total sterol
total *n*-alkanes
µg g^{-1} C
Chl-a (µg m^{-2} d^{-1})
Sep/6 '12 Sep/26 Oct/26 Nov/25 Dec/25 Jan/24 Feb/23 Mar Apr/24 May/24 Jun/23 '13
Start-Date
d.
Net Primary Productivity g C m^{-2} d^{-1}
Sep '12 Oct Nov Dec Jan Feb Mar Apr May Jun '13
Date

Figure 7

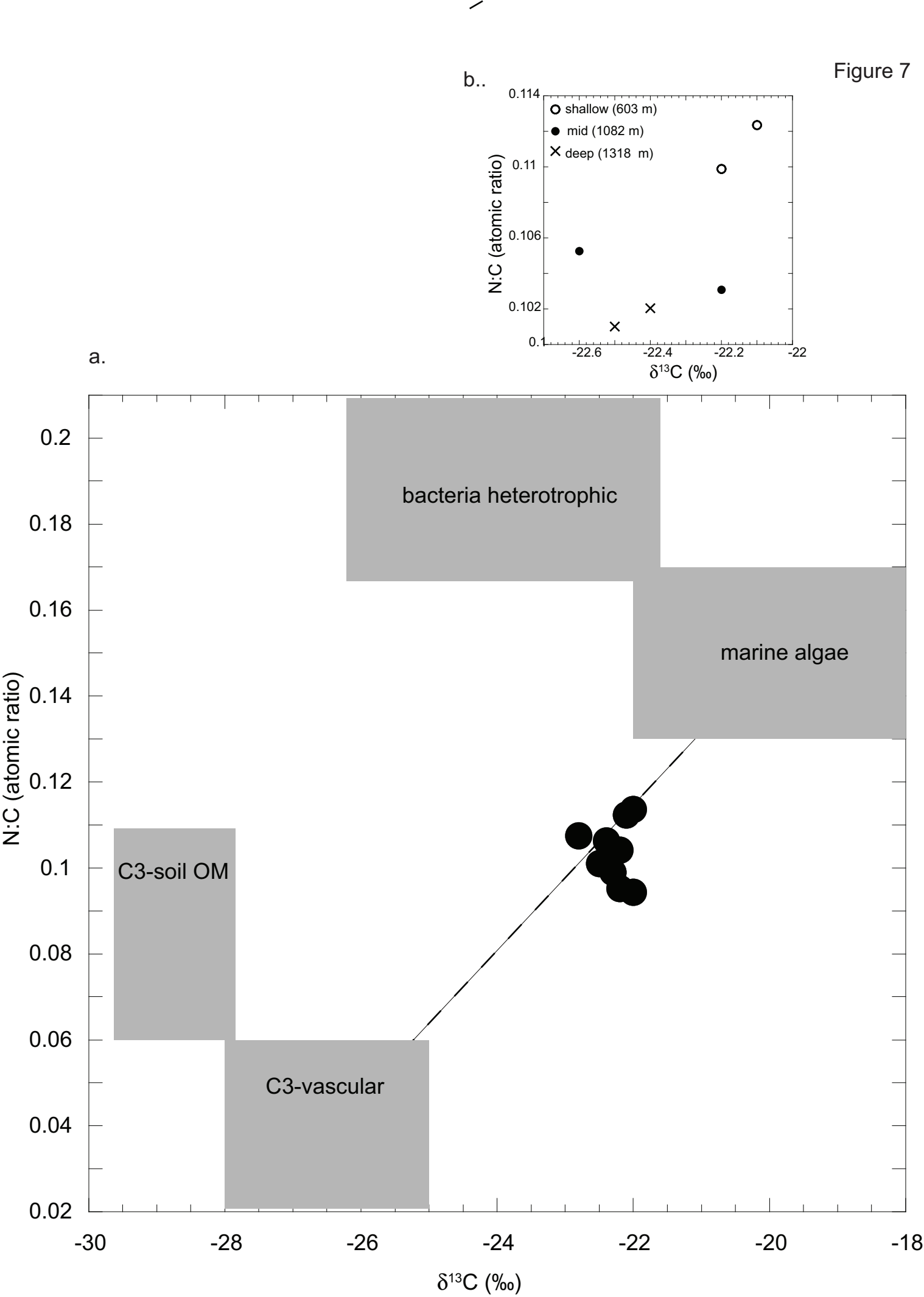
b..
shallow (603 m)
mid (1082 m)
deep (1318 m)
N:C (atomic ratio)
0.114
0.11
0.106
0.102
0.1
-22.6
-22.4
-22.2
-22
δ13C (‰)
a.
bacteria heterotrophic
marine algae
C3-soil OM
C3-vascular
N:C (atomic ratio)
0.2
0.18
0.16
0.14
0.12
0.1
0.08
0.06
0.04
0.02
-30
-28
-26
-24
-22
-20
-18
δ13C (‰)

Start-Date	Mass Flux ($g\ m^{-2}\ d^{-1}$)	N (%)	$\delta^{15}N$ (‰)	C_{org} (%)	$\delta^{13}C$ (‰)	C:N (atomic)	^{210}Pb ($mBq\ g^{-1}$)	Chl-*a* ($\mu g\ m^{-2}\ d^{-1}$)
6-Sep-12	6.7	0.37	5	3.61	-22.4	9.8	1159	0.9
26-Sep-12	9	0.41	5	4.05	-22.5	9.9	1141	4.3
26-Oct-12	5.5	0.41	4.9	3.64	-22.0	8.8	1243	10.5
25-Nov-12	6	0.39	4.9	4.15	-22.0	10.6	1284	3.7
25-Dec-12	7.1	0.39	5	3.74	-22.2	9.6	1184	1.9
24-Jan-13	9.1	0.43	5	3.81	-22.1	8.9	1164	5.4
23-Feb-13	4.7	0.43	4.8	4.32	-22.3	10.1	1268	6
24-Apr-13	2.5	0.41	4.6	4.36	-22.2	10.5	1514	3.1
24-May-13	4	0.42	4.3	3.95	-22.8	9.3	1417	16.1
23-Jun-13	5.4	0.4	4.8	3.75	-22.4	9.4	1296	7.4

Table 1a
Mass fluxes and bulk geochemical measurements from monthly sediment trap samples deployed at 1318 m in Baltimore Canyon, Mid-Atlantic Bight.

Start-Date	Mass Flux ($g\ m^{-2}\ d^{-1}$)	N (%)	$\delta^{15}N$ (‰)	C_{org} (%)	$\delta^{13}C$ (‰)	C:N (atomic)	^{210}Pb ($mBq\ g^{-1}$)	Chl-*a* ($\mu g\ m^{-2}\ d^{-1}$)
7-Sep-12	16.5	0.39	4.9	3.73	-22.6	9.5	890	n/a
26-Sept-12	52.2	0.38	4.9	3.7	-22.2	9.7	713	n/a

Table 1b
Mass fluxes and bulk geochemical measurements from sediment trap samples deployed at 603 m in Baltimore Canyon, Mid-Atlantic Bight.

Start-Date	Mass Flux ($g\ m^{-2}\ d^{-1}$)	N (%)	$\delta^{15}N$ (‰)	C_{org} (%)	$\delta^{13}C$ (‰)	C:N (atomic)	^{210}Pb ($mBq\ g^{-1}$)	Chl-*a* ($\mu g\ m^{-2}\ d^{-1}$)
27-Aug-12	4.5	0.42	4.6	3.85	-22.2	9.1	1107	n/a
26-Sept-12	3.9	0.36	4.9	3.21	-22.1	8.9	1115	n/a

Table 1c
Mass fluxes and bulk geochemical measurements from sediment trap samples deployed at 1082 m in Baltimore Canyon, Mid-Atlantic Bight.

Start-Date	*n*-C_{14}	*n*-C_{15}	*n*-C_{16}	*n*-C_{17}	pr	*n*-C_{18}	ph	*n*-C_{19}	*n*-C_{20}	*n*-C_{21}	*n*-C_{22}	*n*-C_{23}	*n*-C_{24}	*n*-C_{25}	*n*-C_{26}	*n*-C_{27}	*n*-C_{28}	*n*-C_{29}	*n*-C_{30}	*n*-C_{31}	*n*-C_{32}	Σ	CPI	P(aq)
6-Sep-12	n/d	n/d	0.1	n/d	0.09	0.27	0.12	n/d	0.14	0.1	0.16	0.15	0.43	0.36	0.38	0.69	0.46	0.57	0.19	0.19	n/d	4.19	2.42	0.4
26-Sep-12	n/d	0.04	0.03	n/d	n/d	0.08	0.03	n/d	0.04	0.03	n/d	0.06	0.5	0.3	0.7	1.56	1.94	2.55	1.75	1.32	0.53	11.43	5.26	0.09
26-Oct-12	n/d	0.02	0.05	0.03	0.03	0.02	0.07	n/d	0.06	0.04	0.07	0.08	0.07	0.13	0.09	0.15	0.06	0.1	n/d	n/d	n/d	0.97	1.24	0.68
25-Nov-12	n/d	0.02	n/d	0.01	0.01	0.02	n/d	0.03	n/d	0.19	n/d	n/d	n/d	n/d	n/d	n/d	n/d	n/d	n/d	n/d	n/d	0.27	n/a	n/a
25-Dec-12	0.07	0.08	0.06	n/d	n/d	0.05	n/d	n/d	0.04	0.05	n/d	0.07	0.07	0.11	0.06	0.17	n/d	0.2	n/d	n/d	n/d	1.03	2.33	0.47
24-Jan-13	n/d	0.08	0.07	0.04	0.04	0.08	n/d	0.05	0.07	0.06	0.05	0.09	0.07	0.13	0.07	0.18	0.05	0.22	n/d	0.07	n/d	1.38	2.69	0.43
23-Feb-13	0.02	0.06	0.06	0.02	0.03	0.05	n/d	0.03	0.04	0.03	0.05	0.05	3.67	0.08	0.03	0.09	n/d	0.09	n/d	0.04	n/d	4.41	1.63	0.5
24-Apr-13	0.02	0.12	0.1	0.04	0.06	0.07	n/d	0.03	0.08	0.06	0.04	0.05	0.04	0.07	0.01	0.06	0.01	0.07	n/d	n/d	n/d	0.87	1.87	0.63
24-May-13	0.01	0.01	n/d	n/d	0.19	n/d	n/d	0.06	n/d	0.14	0.02	0.21	0.07	0.24	0	0.27	n/d	0.37	n/d	0.19	n/d	1.59	n/a	0.45
23-Jun-13	n/d	n/d	n/d	0.03	0.03	0.02	n/d	0.02	0.01	0.02	0.02	0.06	n/d	0.09	0.02	0.1	0.01	0.1	n/d	0.05	0.01	0.56	7.21	0.5
7-Sept-12[1]	n/d	0.015	n/d	0.014	0.025	0.046	0.013	0.018	n/d	0.022	n/d	0.075	0.166	0.241	n/d	0.255	0.087	0.167	n/d	n/d	n/d	1.11	n/a	n/a
26-Sept-12[1]	n/d	n/d	n/d	n/d	0.026	n/d	n/d	0.048	0.021	0.024	0.034	0.036	0.064	0.042	n/d	0.116	n/d	0.046	n/d	n/d	n/d	0.43	n/a	n/a
27-Aug-12[2]	n/d	0.008	0.004	0.007	0.018	n/d	n/d	0.006	0.009	0.01	n/d	0.025	0.049	0.072	n/d	0.1	0.049	0.06	n/d	n/d	n/d	0.4	n/a	n/a
26-Sept-12[2]	n/d	0.006	0.005	0.008	0.019	0.007	0.008	n/d	0.006	0.009	0.012	0.02	n/d	n/d	n/d	n/d	n/d	n/d	n/d	n/d	n/d	0.07	n/a	n/a

Table 2a

Concentration of total (Σ) and select *n*-alkane concentrations normalized to organic carbon (μg g^{-1} C), and parameters including Carbon Preference Index (CPI), and the Alkane Proxy (P_{aq}) in ~monthly sediment trap samples from the deep site (1182 m). Note: *n/d=below detection limit and n/a=calculation not valid due to n/d values.* $P_{aq}=(nC_{23}+nC_{25})/(nC_{23}+nC_{25}+nC_{29}+nC_{31})$ (Ficken et al., 2000); $CPI=0.5 * [(nC_{25} + nC_{27} + nC_{29} + nC_{31}) /(nC_{24} + nC_{26} + nC_{28}+ nC_{30})] + [(nC_{25} + nC_{27} + nC_{29} + nC_{31})/ (nC_{26} + nC_{28} + nC_{30}+ nC_{32})]$ (Bray and Evans 1961). [1]Data from the shallow (603 m) trap site. [2]Data from the mid-depth (1082 m) trap site. Pr = pristane; ph = phytane

Start -Date	coprostanol	epicoprostanol	5-β-coprostanone	22-dehydrocholesterol	cholesterol	cholestanol	brassicasterol	campesterol	stigmasterol	β-sitosterol	stigmastanol	Σ
6-Sep-12	n/d	n/d	0.72	1.27	3.80	1.21	2.31	0.42	1.10	1.74	1.13	13.71
26-Sep-12	n/d	0.41	0.87	n/d	0.81	n/d	n/d	0.25	0.27	0.83	n/d	3.43
26-Oct-12	n/d	n/d	n/d	3.85	9.02	n/d	6.75	3.61	2.85	3.51	0.89	30.48
25-Nov-12	n/d	n/d	0.34	0.62	2.30	0.57	0.90	0.33	0.71	1.09	0.29	7.16
25-Dec-12	n/d	n/d	0.63	0.67	2.17	0.92	1.10	0.54	1.02	1.31	0.36	8.71
24-Jan-13	n/d	n/d	0.55	6.15	3.01	0.95	2.79	1.05	1.62	2.90	0.58	19.61
23-Feb-13	0.12	0.23	n/d	n/d	0.37	2.36	n/d	0.57	0.27	0.32	0.58	4.82
24-Apr-13	n/d	n/d	0.11	n/d	0.16	0.12	n/d	0.11	0.27	0.20	0.35	1.31
24-May-13	0.13	0.18	0.21	0.94	5.44	8.37	1.44	0.35	1.18	1.52	1.58	21.34
23-Jun-13	n/d	n/d	0.05	n/d	0.28	0.60	0.08	0.10	0.08	0.09	0.07	1.33
7-Sept-12[1]	0.00	0.34	1.15	1.98	10.35	3.30	5.85	2.23	3.46	4.63	2.95	36.23
26-Sept-12[1]	0.05	0.05	0.73	0.30	2.83	1.18	1.84	0.24	0.89	1.48	0.47	10.06
27-Aug-12[2]	0.09	0.00	1.07	0.53	3.99	1.78	2.87	0.38	1.40	2.20	1.46	15.77
26-Sept-12[2]	0.20	0.17	2.05	0.93	7.64	3.40	5.72	0.93	2.99	4.74	2.95	31.73

Table 2b

Concentration of total (Σ) and individual sterols normalized to organic carbon (μg g^{-1} C) in ~monthly sediment trap samples from the deep site (1182 m). Note: *n/d=below detection limit*. [1]Data from the shallow (603 m) trap site. [2]Data from the mid-depth (1082 m) trap site.

Start -Date	%Terrestrial	%Marine	%Anthropogenic
6-Sep-12	40	55	6
26-Sep-12	76	10	14
26-Oct-12	36	63	0
25-Nov-12	35	60	5
25-Dec-12	40	53	7
24-Jan-13	33	64	3
23-Feb-13	38	55	7
24-Apr-13	60	32	8
24-May-13	26	71	3
23-Jun-13	40	55	5
7-Sept-12[1]	37	56	7
26-Sept-12[1]	37	55	8
27-Aug-12[2]	37	59	4
26-Sept-12[2]	31	61	8

Table 3

Major organic matter sources to the sterol and *n*-alkane molecular signatures were investigated by calculating relative proportions of marine, terrestrial higher plants, and anthropogenic/petroleum contributions. Relative contributions from natural (marine versus terrestrial) and anthropogenic organic matter *n*-alkane and sterol sources were calculated following modified designations from Pisani et al. (2013). Terrestrial organic matter composition of sediments was quantified using concentrations of odd-numbered *n*-alkanes in the C_{21} to C_{31} range as well as the sterols campesterol, stigmasterol, β-sitosterol and stigmastanol. Marine components were determined using concentrations of the sterols cholesterol, cholestanol, 22-dehydrocholesterol, and brassicasterol as well as odd- and even-numbered *n*-alkanes in the C_{14} to C_{19} range. The anthropogenic components were determined using the sterol composition of coprostanol, epicoprostanol, and 5-β-coprostanone and the isoprenoid hydrocarbons pristane and phytane. [1]Data from the shallow (603 m) trap site. [2]Data from the mid-depth (1082 m) trap site.

Start -Date	Al	P	V	Cr	Mn	Fe	Cu	Zn	Sr	Mo	Cd	Cs	Ba	La	Tl	Pb	Th	U
6-Sep-12	58200	837	92.9	69.6	538	33600	29.7	91.4	279	0.66	0.12	4.5	449	31.3	0.51	25.9	9.31	2.05
26-Sep-12	56800	870	92	69.4	530	32700	27.5	85.7	283	0.88	0.14	4.5	415	31.3	0.5	28	9.15	2.16
26-Oct-12	55200	886	89.3	66.9	476	31900	28.3	85	298	1.1	0.15	4.4	418	30.4	0.5	26.8	8.84	2.07
25-Nov-12	57300	841	91.6	69.4	648	3 900	28.5	85.4	298	0.79	0.13	4.5	428	32.3	0.51	28.9	9.38	2.18
25-Dec-12	57000	834	91.1	68.3	696	32800	27.9	84.6	285	0.85	0.1	4.5	424	33.4	0.51	28.6	9.65	2.13
24-Jan-13	54200	872	85.2	67.5	568	31700	25	82.8	266	0.91	0.11	4.3	386	31.6	0.48	28	9.23	2.04
23-Feb-13	56200	943	91.6	73.6	501	33100	29.1	88.9	287	0.96	0.14	4.7	422	32.8	0.5	28.4	9.25	2.16
24-Apr-13	55800	948	90.7	68.2	465	32900	30.7	89.7	318	1.4	0.23	4.7	475	32.6	0.52	29.4	9.44	2.26
24-May-13	56800	859	91.4	69.1	440	33600	30.3	86	306	1.8	0.34	4.8	469	33.5	0.53	28.9	9.3	2.18
23-Jun-13	55800	877	90.9	67.4	405	32600	30	82.5	290	0.88	0.2	4.7	466	32.4	0.5	27.1	8.81	2.04
7-Sept-12[1]	54800	858	89.8	68.4	392	32000	26.9	82.4	264	0.97	0.13	4.4	406	33.8	0.49	23.2	9.17	2.23
26-Sept-12[1]	51900	754	82.3	62.3	424	30500	23.4	77.7	274	0.91	0.11	4.2	408	33	0.49	23.4	9.29	2.26
27-Aug-12[2]	55500	809	90.4	66.8	447	32300	27.8	109	277	0.79	0.13	4.6	436	32.1	0.5	24.5	9.29	2.13
26-Sept-12[2]	56600	830	91.5	69.5	439	33000	29.1	83.8	276	0.77	0.16	4.7	438	32.9	0.51	25.5	9.2	2.2

Table 4

Sediment trap trace element concentrations (μg g^{-1}) in ~monthly sediment trap samples from the deep site (1182 m). Al = aluminum; Ba = barium; Cd = cadmium; Cr = chromium; Cs = cesium; Cu = copper; Fe = iron; La = lanthanum; Mn = manganese; Mo = molybdenum; P = phosphorus; Pb = lead; Sr = strontium; Th = thorium; Tl = thallium; U = uranium; V = vanadium; Zn = zinc. [1]Data from the shallow (603 m) trap site. [2]Data from the mid-depth (1082 m) trap site.

Start -Date	Lab ID	F Modern	Fm Err	CRA (years)	CRA error (years)	$\Delta^{14}C$ (‰)	$\Delta^{14}C$ error (‰)	$\delta^{13}C$ (‰)
6-Sep-12	126887	0.8526	0.002	1280	20	-153.75	2.00	-21.68
26-Sep-12	126888	0.8719	0.0018	1100	15	-134.65	1.80	-21.80
26-Oct-12	126889	0.885	0.0019	980	15	-121.57	1.90	-21.58
25-Nov-12	126890	0.8744	0.0018	1080	15	-132.12	1.80	-21.56
25-Dec-12	126891	0.8713	0.002	1110	20	-135.2	2.00	-21.57
24-Jan-13	126892	0.8805	0.0028	1020	25	-126.07	2.80	-21.59
23-Feb-13	126893	0.8754	0.0019	1070	15	-131.13	1.90	-21.73
24-Apr-13	126894	0.8703	0.0019	1120	15	-136.23	1.90	-21.76
24-May-13	126895	0.8758	0.0018	1070	15	-130.77	1.80	-22.15
23-Jun-13	126896	0.8689	0.0024	1130	20	-137.55	2.40	-21.76

Table 5

Radiocarbon results from sediment trap samples from the deep site (1182 m) with fraction modern (Fm) and Fm error (±), with modern defined as 1950, Conventional Radiocarbon Age (CRA) and CRA age error (years), and radiocarbon ($\Delta^{14}C$; ‰) values.

Figure S1
GC-MS total ion chromatogram (TIC) of sediment trap organic matter extracted and fractionated into F1 n-alkane fraction (131-2: 10.20.2012) and F3 sterol and fatty alcohols fraction (131-6: 2.17.2013**)** extracts. a. aliphatic hydrocarbons, internal standards: 5α androstane b. fatty alcohol/sterol, internal standards: 5α-androstan-3β-ol.

Figure S2
Oceanographic variability in temperature, turbidity and north current speed component for the shallow lander in Baltimore Canyon across two time periods, a. October to November 2012 and b. March to May 2013. Note the mechanism, initially a high turbidity event is followed by approximately 2°C fluctuations in temperature, these spikes are associated with high current speeds.

Station	Sample Type	Depth (m)	%Corg
NF-2012-107	Surface sediment (0−0.5 cm) canyon	283	0.4
NF-2012-114	Surface sediment (0−0.5 cm) canyon	652	0.4
NF-2012-054	Surface sediment (0−0.5 cm) canyon	1180	3.9
NF-2012-065	Surface sediment (0−0.5 cm) slope	170	0.1
NF-2012-070	Surface sediment (0−0.5 cm) slope	515	0.3
NF-2012-084	Surface sediment (0−0.5 cm) slope	990	1.1
NF-2012-091	Surface sediment (0−0.5 cm) slope	1186	1.5

Supplementary Table S1
Surface (0-0.5 cm) sediment samples collected within Baltimore Canyon and adjacent slope and respective percent organic carbon (%Corg).

Sample ID	n-C_{14}	n-C_{15}	n-C_{16}	n-C_{17}	pr	n-C_{18}	ph	n-C_{19}	n-C_{20}	n-C_{21}	n-C_{22}	n-C_{23}	n-C_{24}	n-C_{25}	n-C_{26}	n-C_{27}	n-C_{28}	n-C_{29}	n-C_{30}	n-C_{31}	n-C_{32}	Σ
NF-2012-107	0.49	1.59	0.81	0.78	0.25	1.2	0.44	1.59	1.54	1.32	n/d	0.71	n/d	n/d	n/d	0.61	n/d	0.39	n/d	n/d	n/d	11.03
NF-2012-114	1.96	n/d	3.02	2.65	1.39	2.43	n/d	6.84	4.99	4.79	5.62	13.22	19.32	38.55	44.79	68.61	51.06	71.75	34.55	49.19	14.37	437.71
NF-2012-054	0.12	0.38	0.3	0.43	0.26	0.38	0.32	1.13	0.58	0.63	0.36	0.35	n/d	0.66	0.48	1.08	n/d	0.98	n/d	0.31	n/d	8.19
NF-2012-065	7.38	7.89	4.95	3.9	n/d	4.35	n/d	5.41	5.35	n/d	n/d	n/d	n/d	4.05	n/d	n/d	n/d	n/d	n/d	n/d	n/d	43.28
NF-2012-070	n/d	2.37	2.16	n/d	n/d	2.13	n/d	3.59	3.46	2.67	1.74	n/d	2.41	2.76	n/d	n/d	n/d	n/d	n/d	n/d	n/d	23.29
NF-2012-084	n/d	n/d	13.27	n/d	n/d	18.81	n/d	32.49	30.48	n/d	n/d	n/d	n/d	n/d	n/d	n/d	n/d	n/d	n/d	n/d	n/d	95.04
NF-2012-091	0.34	n/d	1.19	n/d	n/d	1.1	n/d	1.88	n/d	n/d	n/d	n/d	n/d	n/d	n/d	n/d	n/d	n/d	n/d	n/d	n/d	4.51

Supplementary Table S2
Concentration of total (Σ) and select *n*-alkane concentrations normalized to organic carbon (μg g^{-1} C) in surface (0-0.5 cm) sediment samples in Baltimore Canyon and adjacent slope. Note: *n/d=below detection limit*

Sample ID	coprostanol	epicoprostanol	5-β-coprostanone	22-dehydrocholesterol	cholesterol	cholestanol	brassicasterol	campesterol	stigmasterol	β-sitosterol	stigmastanol	Σ
NF-2012-107	n/d	n/d	n/d	n/d	1.4	0.76	1.04	3.84	0.75	0.8	0.49	9.08
NF-2012-114	n/d	0.24	n/d	n/d	1.47	2.98	1	2.42	1.21	1.24	n/d	10.56
NF-2012-054	n/d	n/d	n/d	n/d	0.94	0.49	0.87	0.78	0.08	1.26	0.35	4.78
NF-2012-065	n/d	n/d	n/d	n/d	2.6	0.87	n/d	13.1	4.39	1.5	2.13	24.59
NF-2012-070	n/d	n/d	n/d	n/d	2.38	1.21	1.31	2.08	1.36	1.18	1.42	10.95
NF-2012-084	n/d	n/d	n/d	n/d	n/d	n/d	n/d	n/d	n/d	n/d	n/d	n/d
NF-2012-091	n/d	n/d	n/d	n/d	n/d	n/d	n/d	n/d	n/d	n/d	n/d	n/d

Supplementary Table S3

Concentration of total (Σ) and individual sterols normalized to organic carbon (μg g^{-1} C) in surface (0-0.5 cm) sediment samples in Baltimore Canyon and adjacent slope. Note: *n/d=below detection limit*

Site	%Terrestrial	%Marine	%Anthropogenic
NF-2012-107	46	50	4
NF-2012-114	91	8	1
NF-2012-054	54	42	5
NF-2012-065	40	60	0
NF-2012-070	43	57	0
NF-2012-084	n/a	n/a	n/a
NF-2012-091	n/a	n/a	n/a

Supplementary Table S4

Major organic matter sources to the sterol and *n*-alkane molecular signatures were investigated by calculating relative proportions of marine, terrestrial higher plants, and anthropogenic/petroleum contributions in surface sediment samples in Baltimore Canyon and adjacent slope. Relative contributions from natural (marine versus terrestrial) and anthropogenic organic matter *n*-alkane and sterol sources were calculated following modified designations from Pisani et al. (2013). Terrestrial organic matter composition of sediments was quantified using concentrations of odd-numbered *n*-alkanes in the C_{21} to C_{31} range as well as the sterols campesterol, stigmasterol, β-sitosterol and stigmastanol. Marine components were determined using concentrations of the sterols cholesterol, cholestanol, 22-dehydrocholesterol, and brassicasterol as well as odd- and even-numbered *n*-alkanes in the C_{14} to C_{19} range. The anthropogenic components were determined using the sterol composition of coprostanol, epicoprostanol, and 5-β-coprostanone and the isoprenoid hydrocarbons pristane and phytane. *Note: n/a=Source contributions were not calculated due to non-detect sterol and select n-alkane concentrations (Table S2).*

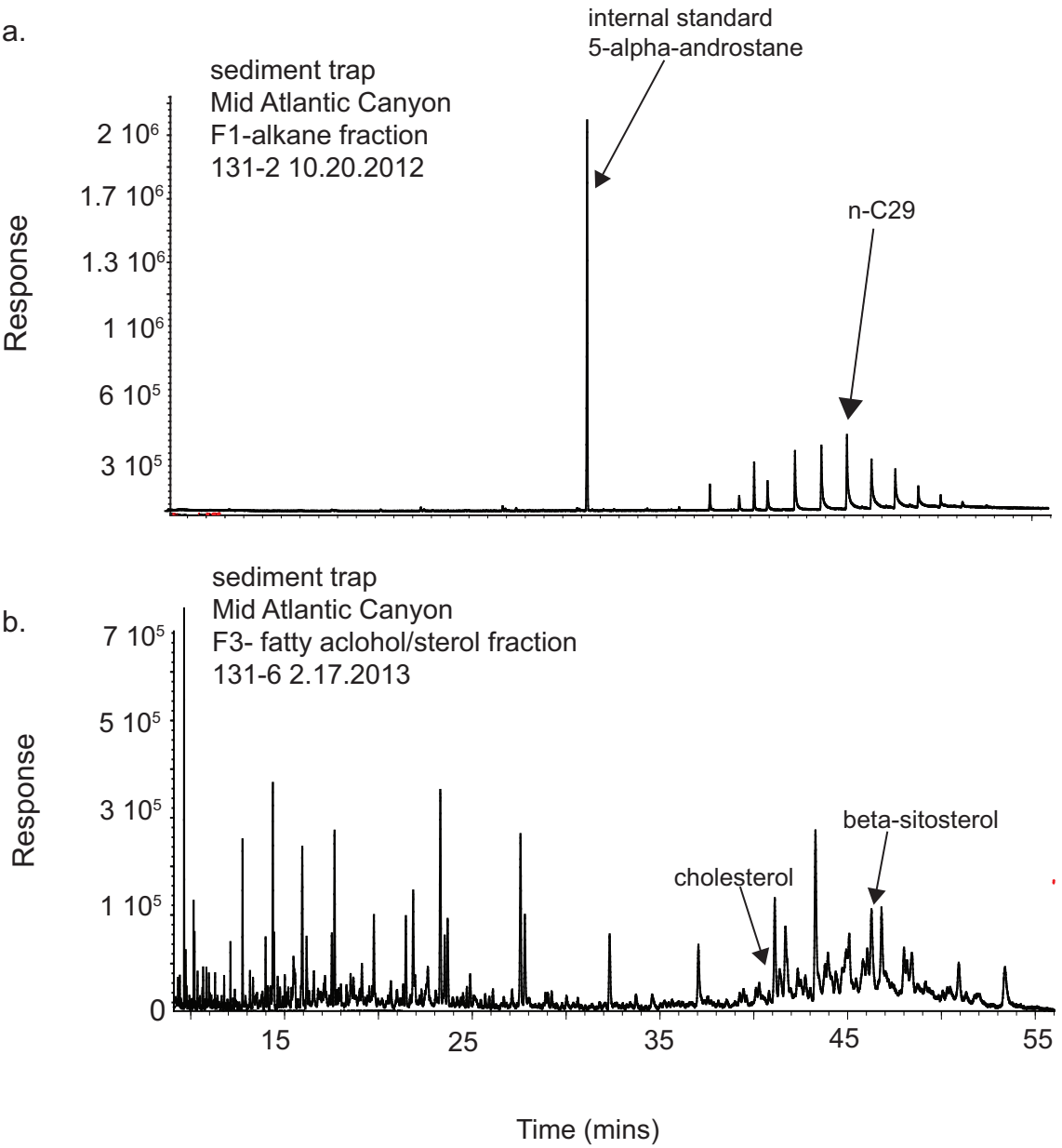
a.
internal standard
5-alpha-androstane
sediment trap
Mid Atlantic Canyon
F1-alkane fraction
131-2 10.20.2012
n-C29
Response
2 10⁶
1.7 10⁶
1.3 10⁶
1 10⁶
6 10⁵
3 10⁵
b.
sediment trap
Mid Atlantic Canyon
F3- fatty aclohol/sterol fraction
131-6 2.17.2013
beta-sitosterol
cholesterol
Response
7 10⁵
5 10⁵
3 10⁵
1 10⁵
0
15
25
35
45
55
Time (mins)

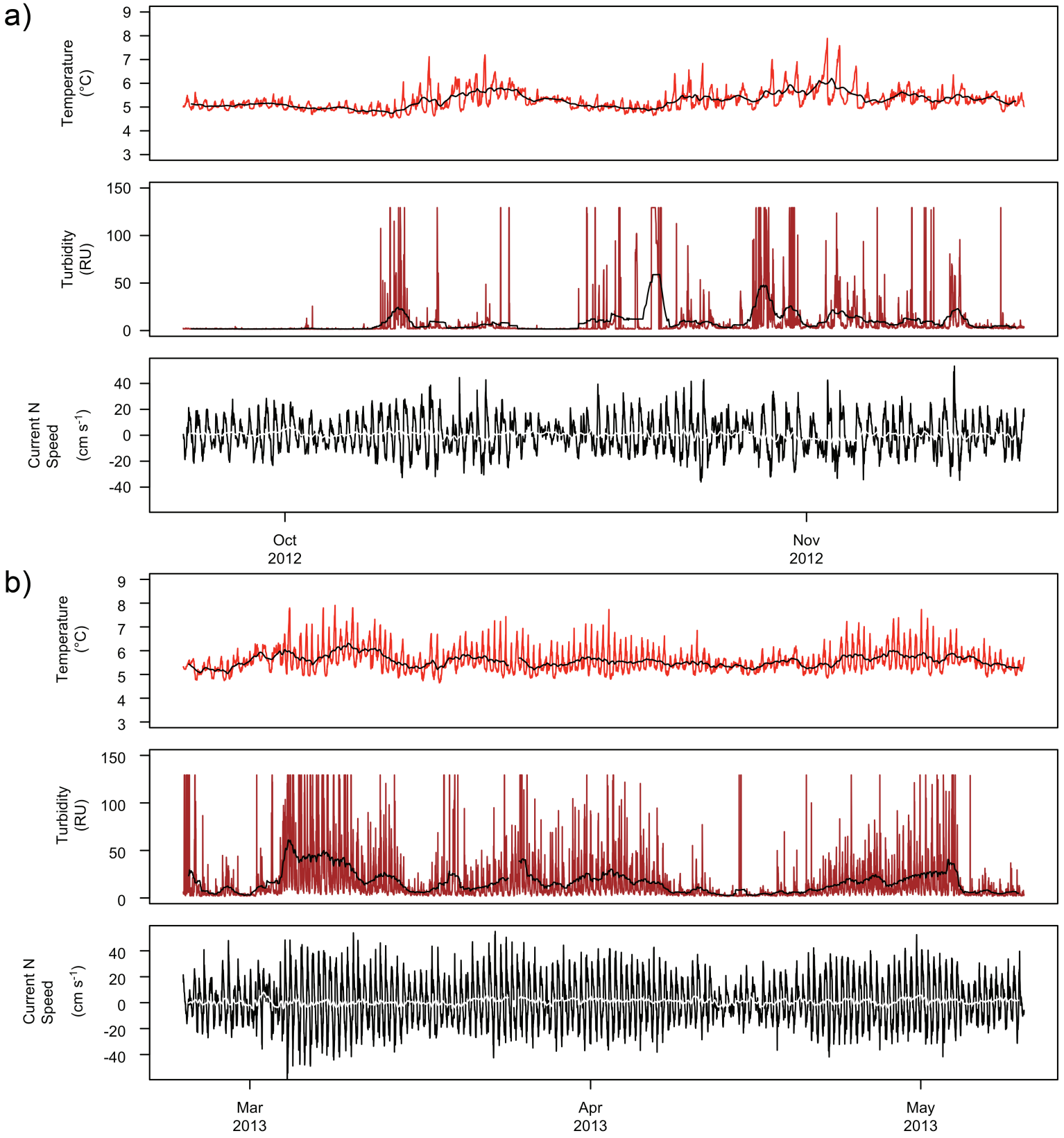
a)
Temperature (°C)
9
8
7
6
5
4
3
Turbidity (RU)
150
100
50
0
Current N Speed (cm s-1)
40
20
0
-20
-40
Oct 2012
Nov 2012
b)
Temperature (°C)
9
8
7
6
5
4
3
Turbidity (RU)
150
100
50
0
Current N Speed (cm s-1)
40
20
0
-20
-40
Mar 2013
Apr 2013
May 2013